AN ABSTRACT OF THE THESIS OF

James Michael York for the degree of Master of Science

in Mechanical Engineering presented on May 13, 1980

Title: THE EFFECT OF ALPHA PHASE MORPHOLOGY ON THE IMPACT ENERGY OF COMMERCIAL PURITY TITANIUM

Abstract approved: Redacted for privacy

William D. McMullen

Samples of commercial purity titanium were heat treated above the beta transformation temperature and within the two phase alpha-beta phase field, followed by cooling at varying rates. Testing of the samples in tension and by instrumented impact indicated that some strengthening could be imparted by these heat treatments, although at a substantial loss in ductility, in some instances. It was found that all of the heat treatment/cooling rate combinations tended to increase the percentage tear energy of the total impact energy. Sevenfold increases in total impact toughness values were observed in some of the samples exhibiting an acicular type microstructure, when the test temperature was increased from 20°C to 100°C. The samples cooled from the two phase region displayed a significantly greater amount of work hardening than that of the annealed material. There was no apparent microstructural reason for this increased work hardening rate.

THE EFFECT OF ALPHA PHASE MORPHOLOGY ON THE IMPACT ENERGY OF COMMERCIAL PURITY TITANIUM

by

James Michael York

A THESIS

submitted to

Oregon State University

n partial fulfillment of
the requirements for the
degree of

Master of Science

Commencement June 1981

APPROVED:

Redacted for privacy

Professor of Mechanical Engineering in charge of major

Redacted for privacy

Head of Department of Mechanical Engineering

Redacted for privacy

Dean of Graduate School

Date thesis is presented May 13, 1980

Typed by Mrs. Connie Schults for JAMES MICHAEL YORK

ACKNOWLEDGEMENT

As is the case with most research endeavors, the production of the final product is not without the assistance, and often the sacrifice, of many individuals. Such is the case for this work.

I wish to express my first thanks to my wife, Barbara, whose patience and tolerance during the attainment of this work is a definite reflection of the strength of our marriage.

For Bill McMullen, my advisor, the contributions and discussions we had were both enlightening and enjoyable. In conducting this research and the analysis to follow, our relationship was more of co-workers than student-teacher.

I wish to acknowledge the long and tedious hours my mother-in-law, Ursula, spent translating a German article for me. It is not without her fanatic accuracy that I could faithfully trust the content of the resultant translation.

I wish to express my thanks to Bill Magedanz for his excellent photographic work, and to Connie Schults for her steadfast determination to translate a maze of corrections into a readable text.

I would like to thank George Dooley and many others at OREMET for supplying the material and assisting in the subsequent production of this work.

Finally, I would like to thank Robert Adrian for his cooperation in the machining of my impact samples.

TABLE OF CONTENTS

LIST OF ILLUSTRATIONS

LIST OF TABLES

THE EFFECT OF ALPHA PHASE MORPHOLOGY ON THE IMPACT ENERGY OF COMMERCIAL PURITY TITANIUM

I. INTRODUCTION

INVESTIGATION BASIS:

If one examines the development of the microstructure-property relationships in titanium and its alloys, it becomes evident that very little work has been done in the field of crack propagation and fracture toughness of the unalloyed grades of titanium. The reason for this apparent informational gap is two-fold. First, the development of fracture mechanics and the subsequent integration of fracture toughness into design criteria were not in existence in the early years of study of titanium as a commercially useful material. Second, although considerable research was conducted to characterize the roles of impurity concentration, microstructure, and environmental effects, on the mechanical properties of unalloyed titanium, it soon became evident that without alloying, titanium had only limited application as a structural material. To maximize the applications of this light-weight metal, particularly for aircraft uses, alloy additions were needed for hardening and strengthening. Subsequent research was almost exclusively focused on titanium alloyed with one or more elements.

As a result of these developments, only a partially complete fracture characterization of unalloyed titanium was conducted. When fracture mechanics and the study of the dynamics of fracture propaga-

tion started to develop, the concepts were applied only to the structural grade alloys.

The purpose of this study is to contribute to the understanding of the room temperature crack propagation characteristics of titanium in the unalloyed state. An attempt will be made to determine the effect of the form of the room temperature alpha phase of titanium on fracture propagation. These results can then be incorporated into the existing knowledge of fracture properties of titanium alloys. By analyzing the characteristics of the alpha phase, present in many titanium alloys, a more exact interpretation can be made of the fracture propagation in multiphase titanium alloys where the alpha phase is only one of the constituents. The frequently encountered statement that unalloyed titanium cannot be strengthened by microstructural manipulation will hopefully be discounted.

BACKGROUND INFORMATION:

Because of the limited scope of this investigation, the best approach for studying the dynamics of fracture initiation and propagation seemed to be by the employment of an instrumented drop weight impact machine. By instrumenting the impacting tup with strain gauges, a near instantaneous load and integrated energy value can be recorded during crack initiation and propagation. The resulting data curves can then be analyzed to determine the percentages of the total energy absorbed by the sample for the various dynamic fracture events. The recent advent of this type of instrumentation does not, as of yet, replace the more expensive sample configurations required for present

fracture toughness measurements as per ASTM E399. However, the additional information generated by instrumenting the impact event gives considerable insight into the fracture process itself. The ability to obtain dynamic fracture data from a relatively simple test employing an inexpensive and traditional geometry sample is quite a revelation in itself.

The room temperature phase composition of unalloyed titanium is in all cases predominately alpha phase. The most common elemental additions or impurities present in unalloyed titanium are: oxygen, nitrogen, carbon, hydrogen, and iron. Only the latter two elements of this list can change the normal phase structure of titanium within the limits of solid solution solubility. Both hydrogen and iron are beta phase stabilizers. For many commercial grades of titanium and titanium alloys, the level of hydrogen content is enough to form titanium hydride needles. This phase forms preferentially to the hydrogen stabilizing the beta phase to room temperature. Craighead has reported a maximum solubility of hydrogen in titanium at room temperature of .0029 $\pm$ .0003 weight percent[1]. Subsequent research by Lenning indicated, however, that at hydrogen contents from the solubility limit to approximately .01 weight percent, the hydride phase in commercial purity titanium was either not observed or indistinguishable from the beta phase retained by the impurity iron[2]. The presence of 0.5 weight percent iron has been postulated by several additional investigators to be sufficient to stabilize the beta phase at room temperature[2,3]. Odinokova and Brusilovskiy determined the presence of both beta phase and the compound TiFe in unalloyed titanium containing only 0.1 weight percent iron in the

annealed state[4]. There is, therefore, strong evidence that the phase composition of unalloyed titanium is of a duplex nature with the possible presence of an additional iron compound and hydride phase under some conditions. The presence of the beta phase is independent of heat treatment while the formation of TiFe may be sensitive to the cooling rate from the elevated temperature beta phase field.

The morphology of the alpha phase in unalloyed titanium can be altered by heat treatment. The typical annealed structure of commercial purity titanium containing oxygen and iron as the principle impurities, is a matrix of equiaxed alpha grains with some intergranular beta. This structure is the result of warm working in both the beta phase field and in the alpha phase field, subsequent to the initial solidification. The final forging sequence must be in the alpha phase field to establish a completely equiaxed structure. By reheating the annealed structure to above the beta transformation temperature, (approximately 925°C but highly dependent on composition) the material reverts to the BCC form. Subsequent cooling from this phase region produces a variety of structures dependent on the cooling rate through the beta to alpha transformation temperature.

Under the action of a rapid water quench, the beta phase transforms martensitically by a nucleation and shear mechanism similar to that occurring in steels[5]. In this instance, however, unlike steels, no supersaturation occurs with respect to the low temperature alpha phase and thus quench strengthening or hardening does not occur[6]. The resultant crystal structure is hexagonal and finely acicular, frequently being referred to as Widmanstätten[7]. The orientation of these Widman-

statten plates often designates the prior beta grain from which they nucleated. The relative fineness of the acicular water quenched structure is significantly affected by composition. Whereas the quenched structure of high purity iodide titanium is more of a serrated type morphology, the addition of oxygen and nitrogen tends to produce and drastically refine the acicular needles[8]. The phenomena of structural refinement by composition will also affect the structures resulting from slower cooling rates.

In general, the net effect of cooling through the beta transformation temperature at progressively slower rates is to gradually coarsen the acicular nature of the alpha structure. At the extreme, Bennett states that holding the martensitic alpha near the transformation temperature for extended periods of time will eventually re-establish the equiaxed annealed structure[9].

The establishment of a completely martensitic alpha structure will hopefully reveal the fundamental differences between it and the annealed structure from the standpoint of fracture propagation characteristics. It would, however, be desirable to reproduce a mixed structure containing both the acicular and equiaxed forms of the alpha phase. Examination of this dual phase structure could then be more directly compared to its counterpart in alpha-beta titanium alloys.

By heating the room temperature annealed structure of unalloyed titanium to just below the temperature of complete transformation to the beta phase, use can be made of the very narrow two phase field to produce a structure containing both the equiaxed and acicular alpha phase morphology. Craighead, et al., and Jaffee, et al., were both successful

in producing a dual phase alpha structure of equiaxed alpha grains and acicular martensitic alpha needles by heat treating near the beta transformation temperature[10,11]. The term "transformed beta" mentioned by both authors is a generic and somewhat ambiguous term used to designate any form of alpha that has transformed from the beta phase. This would be in contrast to alpha formed by nucleation and growth processes.

II. EXPERIMENTAL PROCEDURE

MATERIAL CHARACTERIZATION:

The material used in this investigation was a commercial purity, grade four titanium produced by Oregon Metallurgical Corporation (OREMET). The starting stock was a double melted 76.2 cm diameter ingot reduced approximately 65% in the beta phase region, with the final forging sequence occurring in the alpha phase region at 845°C. The final diameter of the bar stock examined was 5.4 cm.

The chemical composition of the material is given in Table I. As can be seen, the major impurity elements are iron and oxygen, with the hydrogen level being very low at 20 ppm.

The bar, as received from OREMET, had been annealed at 705°C for two hours and air cooled. The microstructure in the longitudinal and transverse directions is shown in Figures 1 and 2. The structure is essentially equiaxed alpha phase with a distinct elongated and oriented shape in the direction of working. The mean grain diameter as determined by the intercept method is 0.40 mm. The darker phase visible is probably beta phase, but could contain some of the compound TiFe. The light etching intragranular phase may be more of the beta constituent only slightly attacked by the etchant or perhaps more alpha with a somewhat different nucleation history than that of the bulk of the matrix.

The average hardness of the annealed structure from four separate determinations was HRB 98.

TABLE I. CHEMICAL COMPOSITION OF MATERIAL STUDIED.

Element	% Content By Weight
C	0.018
N	0.009
O	0.40
H	0.002
Fe	0.350
Other Elements	<0.40 Total

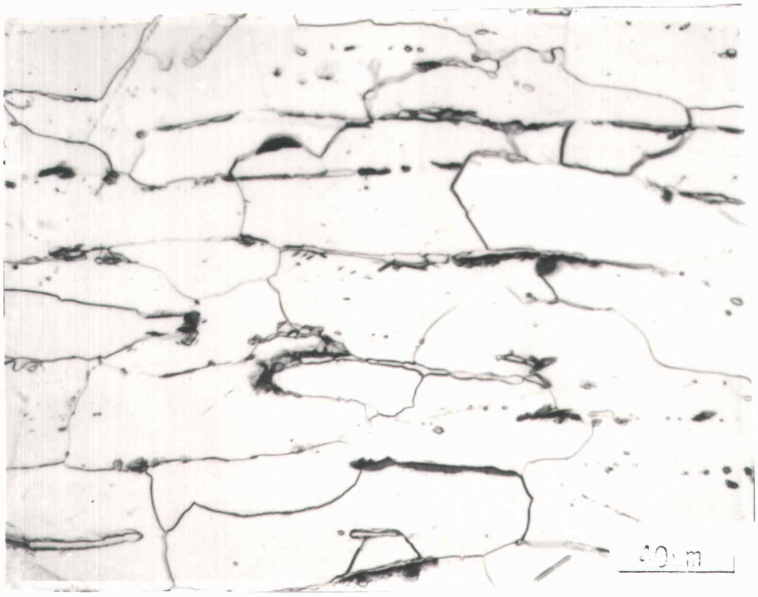

Figure 1. Longitudinal microstructure of starting material, 400X.

Figure 2. Transverse microstructure of starting material, 400X.

HEAT TREATMENT:

The temperature of the alpha to beta phase transformation was determined metallographically. Coupons measuring 12mm X 12mm X 18mm were heated in a furnace to temperatures between 915°C and 954°C, held for 45 minutes at temperature, and then quenched in water, sectioned, polished and examined. The actual point of complete transformation was based upon the appearance of a totally acicular or Widmanstätten structure with no presence of primary alpha. The temperature of complete transformation was approximately 940°C with the two phase region extending down to approximately 930°C. Each sample examined was sectioned in the middle of the 18 mm dimension and polished on the abrasive saw cut face to preclude any misinterpretations from oxygen or nitrogen contamination stabilizing the alpha phase to a higher transformation temperature than the bulk material.

To produce microstructures displaying a completely acicular type morphology, heat treatments were conducted at the lower end of the beta phase field at 982°C. A total of 15 oversized and unnotched Charpy impact specimens and six oversized tensile specimens were heated in a muffle furnace under oxidizing conditions to 982°C and held for one hour at temperature. Five Charpy specimens and two tensile bar specimens were cooled at each of the following rates: (1) quenched in water held at 10°C, with an average cooling rate of 32°C/sec, (2) air cooled, 1°C/sec on the average, and, (3) furnace cooled, 0.1°C/sec, on the average.

For the mixed or dual phase microstructures, heat treatment was conducted at a maximum temperature of 934°C for one hour before quenching a

set of seven samples at each of the above cooling rates. The temperature cycling of the furnace resulted in the controller temperature setting of 920°C varying plus or minus 13.5°C. This constant thermal cycling coupled with the inherent narrowness of the alpha-beta phase region for commercial purity titanium, resulted in structures that did not represent equilibrium phase distributions. All of these samples were cycled between regions of predominantly acicular structure and equiaxed structure. In addition, variations in temperature within the furnace enclosure of plus or minus 5.5°C led to some variability in the percentage of microconstituents between samples. Allowances were made for this variation in analyzing the results. The same thermal cycling mentioned above also was present during the heat treatments in the beta phase field. In this instance, the maximum temperature was 996°C. Aging treatments were not conducted on any of the samples.

METALLOGRAPHY:

Samples for microstructural examination were taken from the ends of the Charpy impact bars after heat treatment and examined in both the longitudinal and transverse directions. Each sample was prepared by the following sequence: sectioning by water cooled abrasive saw, mounted in Bakelite, ground on wet 120, 240, 400, and 600 grit papers or belts, polished on wheels coated with six micron diamond, 0.3 micron levitated alumina in deionized water, and 0.05 micron alumina levitated in deionized water, the latter two steps employing synthetic rayon napped polishing cloths. The final polishing step was conducted with the addition of a solution of 0.5% hydrofluoric acid, 1% nitric acid, and

water, applied directly to the polishing wheel during polishing. All samples were etched with Kroll's etchant; 1% hydrofluoric acid, 2% nitric acid, and water, for periods of 15 to 20 seconds by swabbing.

Examination was conducted on an inverted stage Olympus metallograph employing both brightfield and polarizing illumination.

MECHANICAL TESTING:

Two samples from each particular combination of heat treatment and cooling rate were machined into standard size threaded end tensile bars with a one inch gage length and 0.250 inch gage diameter according to ASTM E8[12].

Tensile testing was conducted on an Instron model TTC. Samples were tested at a crosshead rate of 0.02 min^{-1} until general yielding occurred, when the crosshead rate was then increased 10 to 20 times to insure total fracture in approximately one additional minute. Yield strength was determined by the usual 0.2% offset method and elongation and reduction of area determinations were by conventional sample dimensioning.

The remaining five samples from the individual sets of heat treatments and cooling rates were machined into standardized Charpy V notch impact samples according to the ASTM specification E23[13].

Impact testing was conducted on a drop weight impact machine with Dynatup instrumentation by Effects Technology Inc., Santa Barbara, California. A strain gage resistance bridge is incorporated into the impacting tup to instrument the impact event. A fiber optic bundle and flag assembly on the column of the instrument are used to sense the falling head prior to impact. During impact, an electrical signal is sent

from a velocometer to the time base of a Tektronix series 5100 storage oscilloscope. The DC voltage signal from the strain gages amplified by a dynamic response module produces a load-time plot of the tup loading during the impact. An integrated energy-time curve is also produced at the same time. The storage scope allows both line traces to be preserved so that a photographic record can be made. The load-time curve units can be read directly depending on the setting of the dynamic response module and the oscilloscope sweep rate. Any particular value of the integrated energy curve must be corrected mathematically to represent energy absorbed by the sample during crack initiation and propagation. To standardize the initial energy of the tests, all drops were made from a one foot drop height.

Three of the five machined impact samples for each heat treatment and cooling rate were tested at room temperature, 20°C. The remaining two samples were tested after holding for one hour in boiling deionized water at 100°C. The time span between removal of the sample from the bath and contact with the tup was two to three seconds.

SCANNING ELECTRON MICROSCOPY:

Examination of the representative fracture surfaces from both the tensile specimens and impact specimens for each combination of heat treatment and cooling rate were examined on an ISI Minisem scanning electron microscope. The accelerating voltage was 15 KV and sample manipulation was by a triaxial goniometer. Because of the small specimen chamber on this particular instrument, the fracture surfaces were sectioned by hand from the broken sample halves before examination.

III. MICROSTRUCTURAL VARIATIONS

TRANSFORMED STRUCTURES:

All of the samples heat treated above the alpha-beta phase transformation temperature displayed varying degrees of acicularity or serration.

The microstructure produced by water quenching from the beta phase field is shown in Figure 3. The structure is a very fine network of Widmanstätten needles oriented somewhat randomly, with a fine distribution of the beta phase at the needle boundaries. Although this high magnification micrograph does not show it, the general orientation of the needles reflect the prior beta phase grain size with bulk needle orientation changing at the beta grain boundaries. Examination of the structure at 1000X failed to reveal any of the detail of the beta phase. The fine acicular structure is quite characteristic of the martensitic type transformation of commercial purity titanium as well as many of the alloys of titanium. Due to the rather gross amount of microstructural alteration in transformations from the beta phase, the oriented grain structure visible in Figure 2 is no longer discernable.

By cooling at a somewhat slower rate from the beta region, the resultant alpha phase structure is significantly different from the water quenched morphology. The air cooled structure is shown in Figure 4. In this instance, the alpha is best described as moderately acicular. The general orientation of the acicular needles is reminiscent of the finer quenched structure and the retained beta phase still lies between the individual needles. It seems unlikely that either this structure or the

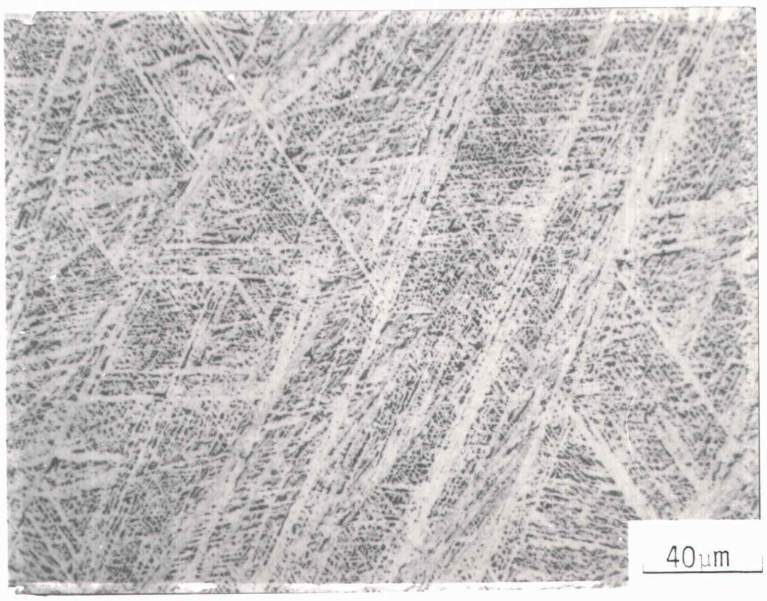

Figure 3. Microstructure resulting from water quenching from the beta phase field, transverse direction, 400X.

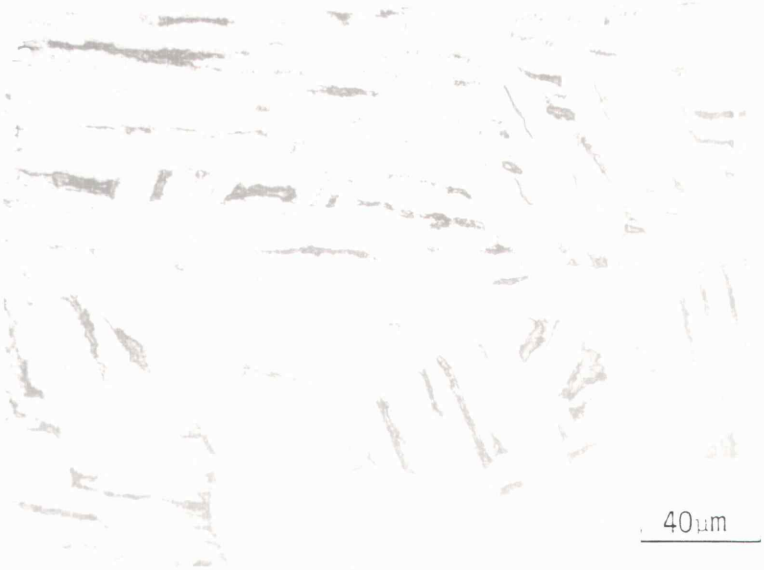

Figure 4. Coarse acicular structure resulting from air cooling from the beta phase field, transverse, 400X.

water quenched structure contains any of the compound TiFe because the relatively rapid cooling rates would not allow for much diffusion. Although the beta phase occupies essentially the same locations as in the water quenched form, its distribution seems to be more limited, and some coalescence or growth has occurred in the relative size of each individual beta region.

When the cooling rate from the beta phase region is slow enough, it begins to approximate equilibrium conditions. This circumstance is apparent in the furnace cooled structure shown in Figure 5. The acicular needles in this micrograph are seen to have coarsened significantly. The morphology approached that of the annealed structure in some regions not shown in the figure. The beta phase is seen to have preferentially formed along most of the individual needle boundaries. The variable tones of this darker etching phase may indicate that the structure is possibly duplex with some of the compund TiFe present. The conditions leading to the development of this compound would certainly be approached by the slow cooling rate. The inter-needle beta phase is not continuous however, with numerous regions of the structure no longer exhibiting parallel clusters of needles, thereby disrupting the pattern of the beta and TiFe phases. The width of these coarse needles exceeds the mean grain diameter of the annealed structure by approximately 10%.

MIXED PHASE STRUCTURES:

Problems were encountered in controlling the relative amounts of each phase between samples in heat treating the samples in the two phase alpha-beta region. Figure 6 represents the structure developed in the

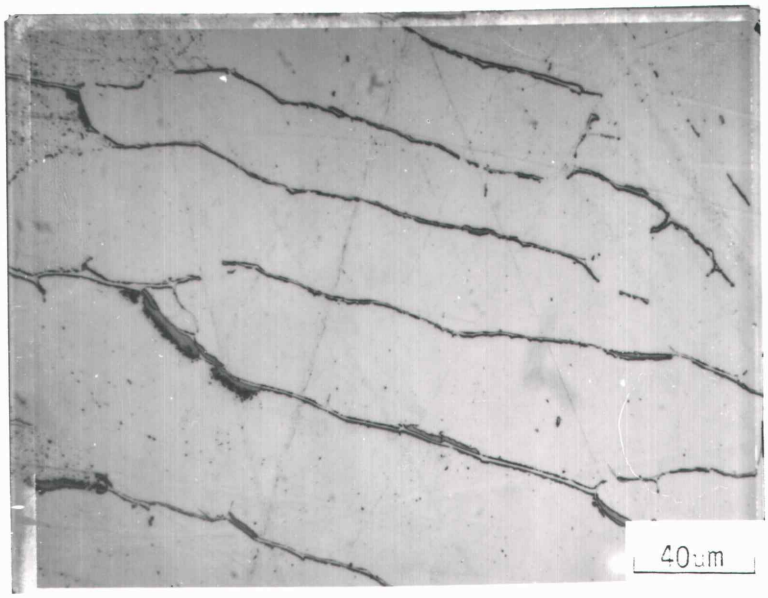

Figure 5. Coarse columnar type structure produced by furnace cooling from the beta phase region, transverse, 400X.

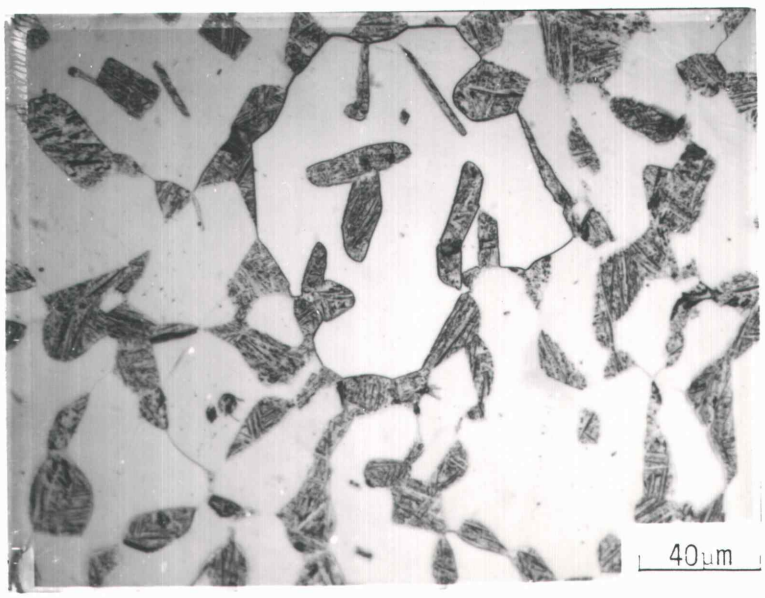

Figure 6. Mixed phase structure resulting from water quenching from the two phase field. Microstructure is approximately 30% acicular alpha, transverse, 400X.

lower portion of the two phase region followed by water quenching. The amount of acicular alpha is approximately 30%. Variations in temperature within the furnace enclosure, however, allowed structures representative of the upper portion of the two phase region to develop. Figure 7 shows a water quenched structure estimated to have reached a temperature 8.5°C higher than that of Figure 6. In this instance, the major constituent has changed from the equiaxed alpha structure to the acicular transformed alpha and beta structure. In Figure 7, the amount of equiaxed or primary alpha is approximately 35%. In both structures, it appears that as the alpha-beta transformation temperature is approached, the grain boundary regions of the equiaxed alpha are the first to transform to the beta phase. As the temperature is increased, transformation begins to occur within the alpha grains in addition to the grain boundary reactions. The transformed structures resulting from water quenching from the two phase field appear to be essentially identical to those produced by water quenching from the beta phase region. As the percentage of transformed structure increased in these microstructures from the two phase region, the directionality of the annealed alpha became less apparent.

The problem of variable phase proportions was less pronounced in the air and furnace cooled samples. Figure 8 is the typical structure resulting from air cooling from the two phase region. The structure is predominantly primary alpha with small regions of beta or transformed structure. The small amount of this second phase, less than 10%, and its distribution in the matrix, indicates that the expected air cooled acicular structure did not develop. It is possible that with the slower

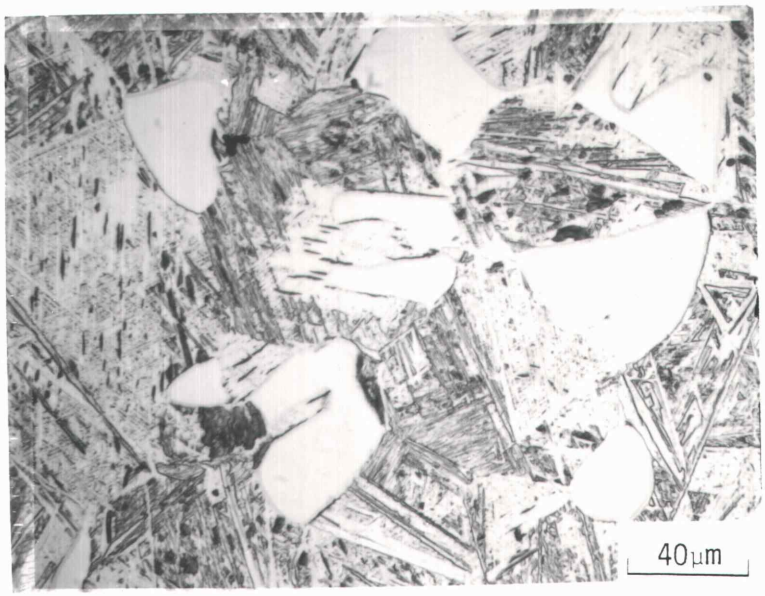

Figure 7. Microstructure resulting from heating 8.5°C higher than in Fig. 6 before water quenching. Transformed structure is now approximately 70% of field of view, transverse, 400X.

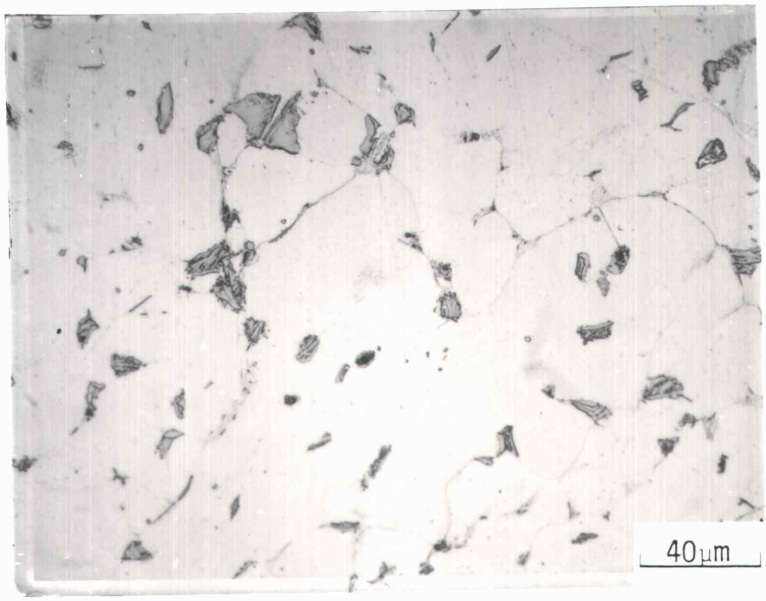

Figure 8. Microstructure resulting from air cooling from the two phase field, transverse, 400X.

cooling rate, some of the transformed alpha becomes incorporated into the equiaxed alpha grains. The second phase observed in this micrograph, then, could be assimilated beta phase. This observation would certainly be consistent with that of the air cooled structure from the beta phase region. In both instances, the amount of transformed alpha is significantly greater than the amount of retained beta. The subtle acicular pattern in the beta phase observed in Figure 8 may be the result of a combination of beta and TiFe. In comparing the distribution and population of the beta phase here with that of the annealed structure, there seems to be a significant reduction in the population of beta particles and a definite increase in their relative size. Although the overall structure in this micrograph has coarsened relative to the annealed structure, the directional grain orientation was still visible when this sample was examined in the longitudinal direction.

The structure resulting from furnace cooling from the two phase region is very similar to that resulting from air cooling. The structure, shown in Figure 9, consists of equiaxed alpha grains and a somewhat greater amount of beta phase, 15 to 20%. In addition, the beta phase in this sample has assumed a serrated morphology. The fine dispersion of particles within the grains may be partially attributed to the compound TiFe, although the majority of them are considered to be the result of staining or pitting from the etchant. The lighter appearing structure within the beta regions has the general shape of grain boundaries and triple point grain intersections, and is therefore, likely to be the transformed alpha phase. However, this same structure was observed in the air cooled samples with a less developed shape, and

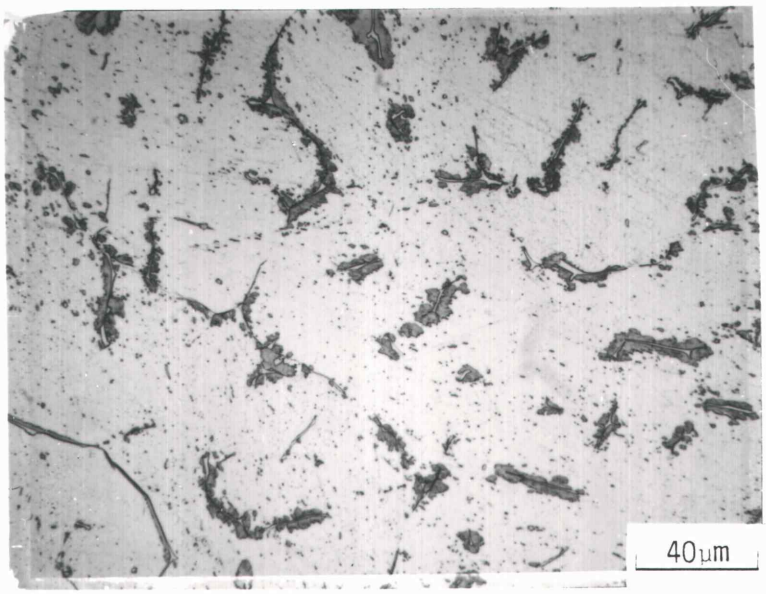

Figure 9. Microstructure resulting from furnace cooling from the two phase field, transverse, 400X.

was attributed to the compound TiFe. Since the grain boundaries and grain intersection points are likely spots for either transformed or acicular alpha and TiFe formation, an exact identification cannot be made optically. Examination of other samples with this same heat treatment and cooling rate indicate that the amount of beta phase present may vary from 5% to 20% between any two of the seven samples.

IV. MECHANICAL PROPERTY RESULTS: TENSILE TESTS

All of the tensile testing was conducted at room temperature. The strain rate employed was 0.02 min^{-1}. This value is slightly higher than the value 0.005 min^{-1} generally called out in titanium material specifications, but the difference was less than one order of magnitude. Although titanium is strain rate sensitive, this small difference in strain rate from established practice was felt to be insignificant with regard to its effect on either the strength or tensile ductility of the samples. The tensile test results from all six of the various combinations of heat treatment and cooling rate, as well as those of the annealed material, are shown in Table II. Also included in Table II are the average Rockwell "B" hardness values (HRB) determined from four separate readings on one representative sample from each heat treatment. Due to operator error and limited material availability, only one tensile test was conducted on the annealed material.

Probably the most significant observation that can be made with regard to the more historical misconceptions about commercial purity titanium is that it can, in fact, be somewhat hardened by heat treatment. Examination of the ultimate strength, yield strength, and hardness of the two sets of samples that were water quenched indicate measurable increases over that of the annealed material. Ultimate strength was increased up to 10%, yield strength up to 13%, and hardness was increased some five points on the Rockwell "B" scale. The largest increases in strength and hardness came from the completely acicular structure of the samples quenched from the beta phase field. However,

TABLE II. TENSILE TEST RESULTS

Heat Treatment	Ultimate Strength MPa	Yield Strength MPa	Spread Between Ultimate and Yield Strength MPa	Elongation (%)	Reduction of Area (%)	Hardness HRB
705°C for 2 hr.* -Air Cool	707	572	135	25.0	42.1	98.4
982°C for 1 hr.	783	667	117	3.0	4.0	103.0
-Water Quench	770	646	124	3.5	5.5	(25.5HRC)
982°C for 1 hr.	721	581	141	14.5	14.6	93.2
-Air Cool	665	570	95	9.5	13.1	
982°C for 1 hr.	680	554	126	6.5	7.1	90.5
-Furnace Cool	673	554	106	4.5	7.1	
920°C for 1 hr.	730	553	177	21.5	37.2	95.7
-Water Quench	748	587	161	23.5	39.0	
920°C for 1 hr.	650	433	217	22.0	30.2	87.3
-Air Cool	656	433	223	23.0	33.3	
920°C for 1 hr.	676	503	173	22.5	34.7	94.6
-Furnace Cool	691	511	180	24.5	34.0	

*Material in as received condition.

some improvement in properties also occurred in the samples where the acicular alpha morphology was only a portion of the total phase composition of the microstructure. The strength increases observed in Table II appear to have developed at a sacrifice in ductility of those samples cooled from the beta phase field. Both the water quenched and furnace cooled samples exhibit minimal elongation and reduction of area values. The same lack of ductility is not noted in the mixed phase samples where the acicular structure was only one of the phase constituents.

The general trend in strength and hardness for those samples cooled from the beta phase field is that of decreasing property magnitude as the cooling rate increases. This trend results in the furnace cooled samples exhibiting lower properties than that of the annealed material. An inversion of the above trend occurs, however, with respect to the ductility of these six samples. For no obvious reason, the air cooled samples have two to three times the ductility of the water quenched or furnace cooled samples. An explanation for this anomaly is not readily apparent. This particular structural form, however, does lie between two other microstructural extremes. On the one hand, the water quenching produces a rather drastic change in morphology which may be of inherent low ductility, while on the other hand, the very slow cooling rate of the furnace cooled samples would tend to maximize any precipitational processes that could be detrimental to ductility.

A different trend in property results is noted for the mixed phase samples. For these samples, an inversion seems to occur in the air cooled results. Whereas there is a decreasing trend from the water quenched to the furnace cooled samples, the air cooled samples exhibited

lower tensile strength, yield strength, and hardness than either of the other two cooling rates, and in fact, exhibited the lowest strength values in this study. This same tendency is not apparent in the ductility results, which vary only slightly. It is quite significant that the anomalous tensile test results occurred with air cooling in both heat treatments.

Another interesting observation can be made when one examines all of the tensile test results with regard to the difference or spread between the ultimate strength and the yield strength. This difference is basically constant for the annealed structure and for those samples cooled from the beta region. However, this difference is only from 50% to 75% of the differences between strength values for the mixed phase samples. Since the ultimate strengths for these latter samples are in some instances greater, and in other cases less than that of the annealed material, it becomes apparent that the mixed phase structures exhibit significantly lower yield points. This increase in the amount of load required to cause total fracture over that of the other structures indicates that the mixed phase microstructures exhibit a greater degree of work hardening without any detrimental effects in the final ductility parameters. This increase in spread between strength values of the mixed phase samples cannot be the result of a strain rate effect since all of the samples tested were strained at the same rate, even after general yielding had occurred. A general reduction in strength as a result of heat treatment within the two phase region would not be expected to affect the yield strength without decreasing the ultimate strength a proportionate amount.

A graphical representation of the data in Table II is shown in Figures 10 and 11. All of the strength and hardness values tend to follow the same general pattern. The elongation and reduction of area graphs are also of similar form but with approximately the same difference in magnitude for the mixed phase samples as that observed for the annealed structure. The previously mentioned inversion in strength values for the air cooled dual phase samples is readily apparent in Figure 10. The increased difference between the ultimate strength and yield strength graphs for all of the dual phase structures is also quite noticeable.

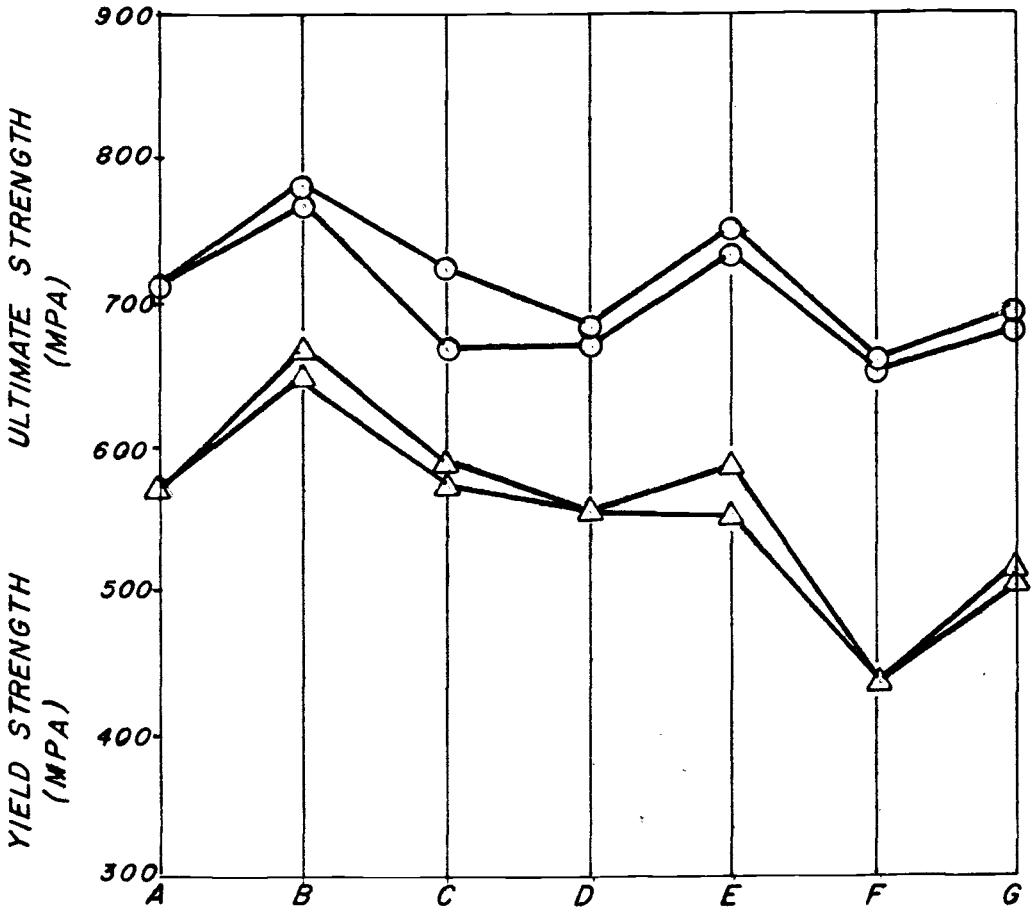

Figure 10. Effect of heat treatment and cooling rate on tensile and yield strength.
A = 705°C-2hr/A.C., B = 982°C-1hr/W.Q.,
C = 982°C-1hr/A.C., D = 982°C-1hr/F.C.,
E = 920°C-1hr/W.Q., F = 920°C-1hr/A.C.,
G = 920°C-1hr/F.C.

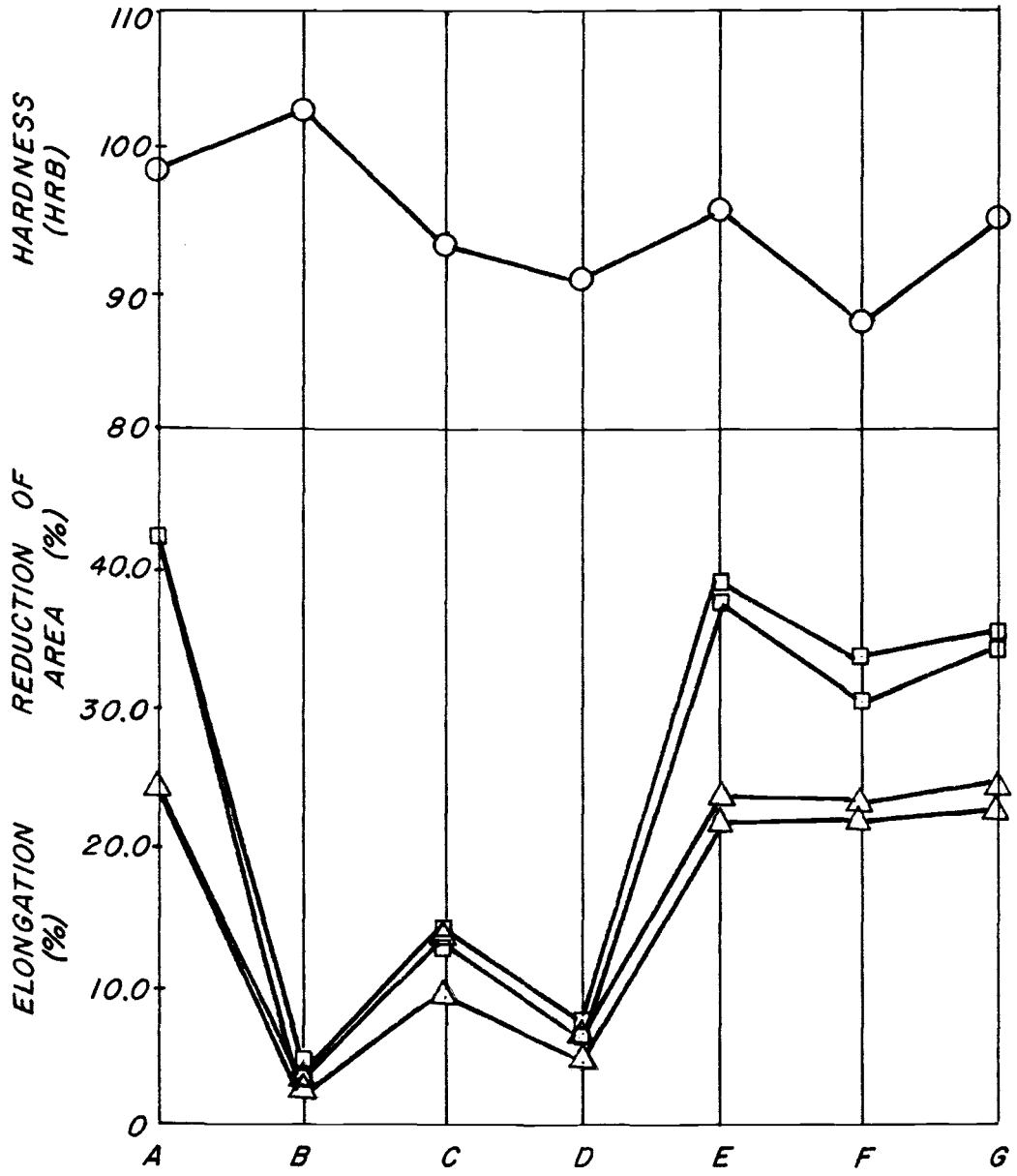

Figure 11: Effect of heat treatment and cooling rate on ductility and hardness. A = 705°C-2hr/A.C., B = 982°C-1hr/W.Q., C = 982°C-1hr/A.C., D = 982°C-1hr/F.C., E = 920°C-1hr/W.Q., F = 920°C-1hr/A.C., G = 920°C-1hr/F.C.

V. MECHANICAL PROPERTY RESULTS: IMPACT

The drop weight frame and related instrumentation used for the instrumented impact testing of the Charpy samples is shown in Figure 12. The control unit for releasing the drop weight is to the right in the photo. The oscilloscope and dynamic response module are situated at the left. Figure 13 shows the fiber optics and flag assembly at the lower right side of the column and a closer view of the impacting tup. The light imput from the fiber optic bundle goes to a velocometer at the rear left of the column, which then generates a voltage signal for the time base of the oscilloscope. A brake assembly and switch are located on the column stantions and frame respectively, and upon activation during sample impact, are delay activated to brake the drop head and prevent bouncing.

Although the instrumentation as shown in Figure 12 yields both a load-time curve and an integrated energy-time curve, it was felt that a more reliable and accurate representation of the sequential initiation and fracture energies could be obtained from the load-time curve alone. A typical load-time plot for an impact test of a ductile material is shown in Figure 14. The initial linear rise of the curve is not unlike that that occurs during the early portion of a tensile test, and as such represents an elastic response of the sample. The energy absorbed by the sample to this point, as determined by the area under this portion of the curve, is designated as the elastic energy (E_A). The portion of the curve adjacent to the linear segment is shown as a gradual rise in

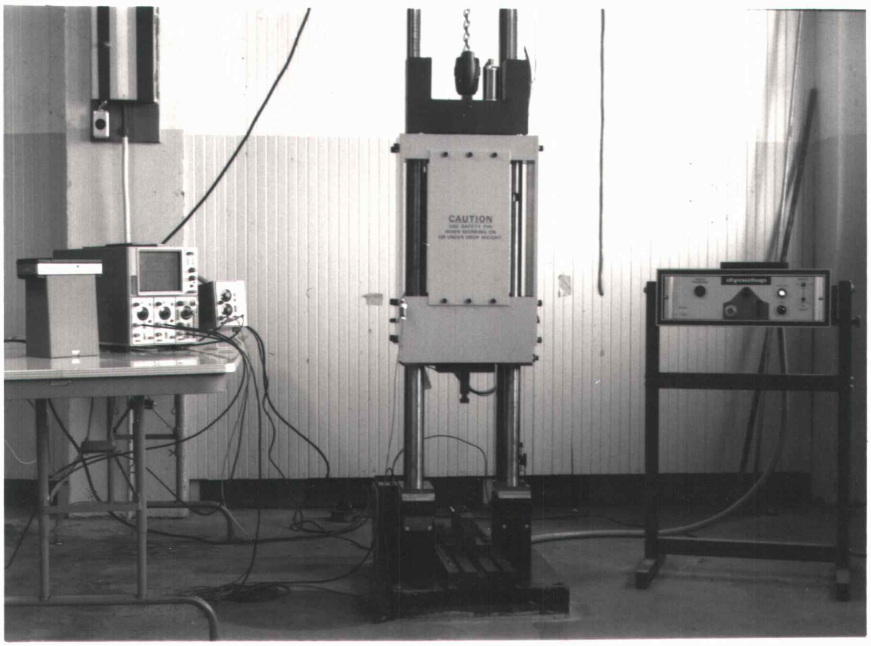

Figure 12. Equipment set-up for instrumented impact testing.

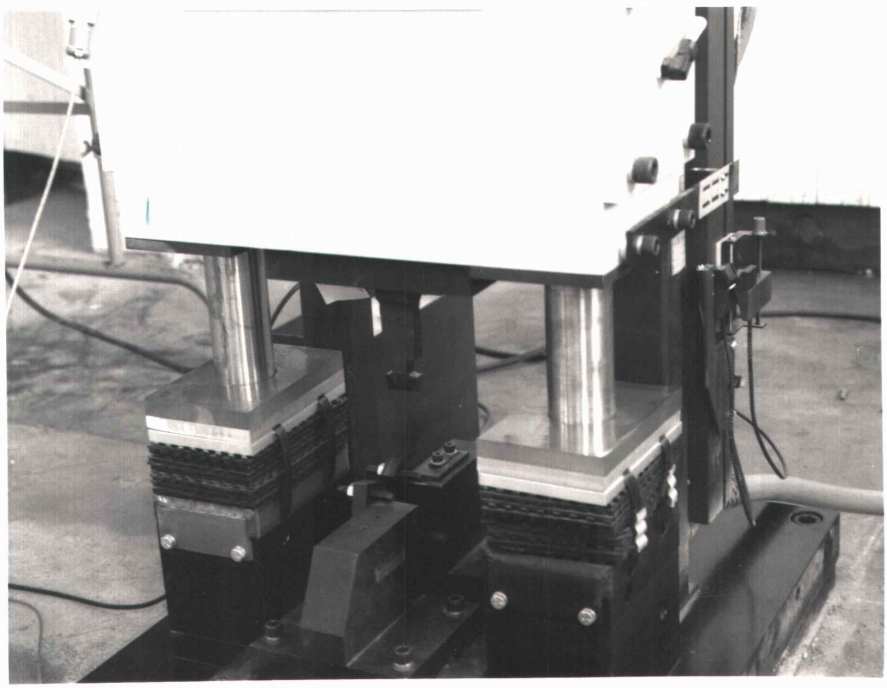

Figure 13. Closer view of lower portion of drop tower showing fiber optic-flag assembly (to right of column), and impacting tup.

load and then the beginning of load drop off. The area under this curve portion represents the balance of the energy required to initiate a crack in the sample. This area will be referred to as the initiation energy (E_B), and is often a significant portion of the total energy absorbed by the sample. The rather sudden drop off in load after crack initiation is associated with the sudden instability of the crack referred to as a crack pop-in, and the resultant energy increment is the pop-in energy (E_C). The final portion of the curve represents the propagation of the crack across the sample. The area under this region of the plot is the tear energy (E_D). The amount of tear energy relative to the total energy absorbed by the sample gives some added insight into the fracture toughness of the sample tested.

For all of the samples tested, the load-time plots were divided into the four areas shown in Figure 14. Each area was determined by tracing with a planimeter. The resultant areas were then multiplied by the scale factors for the time and load axes and corrected to give the energy absorbed by the sample[1]. In some instances, the load-time plot was such that the smaller areas representing the elastic energy and pop-in energy could not be determined.

Figures 15 thru 21 are slightly reduced representations of the load and energy traces off of the photographically recorded oscilloscope displays for typical test samples tested at 20°C and 100°C. In all cases, the vertical scale was 6.89 MPa per grid division and the horizontal scale was either 0.1, 0.2, or 0.5 msec per grid division. It should be

---

[1] See Appendix A

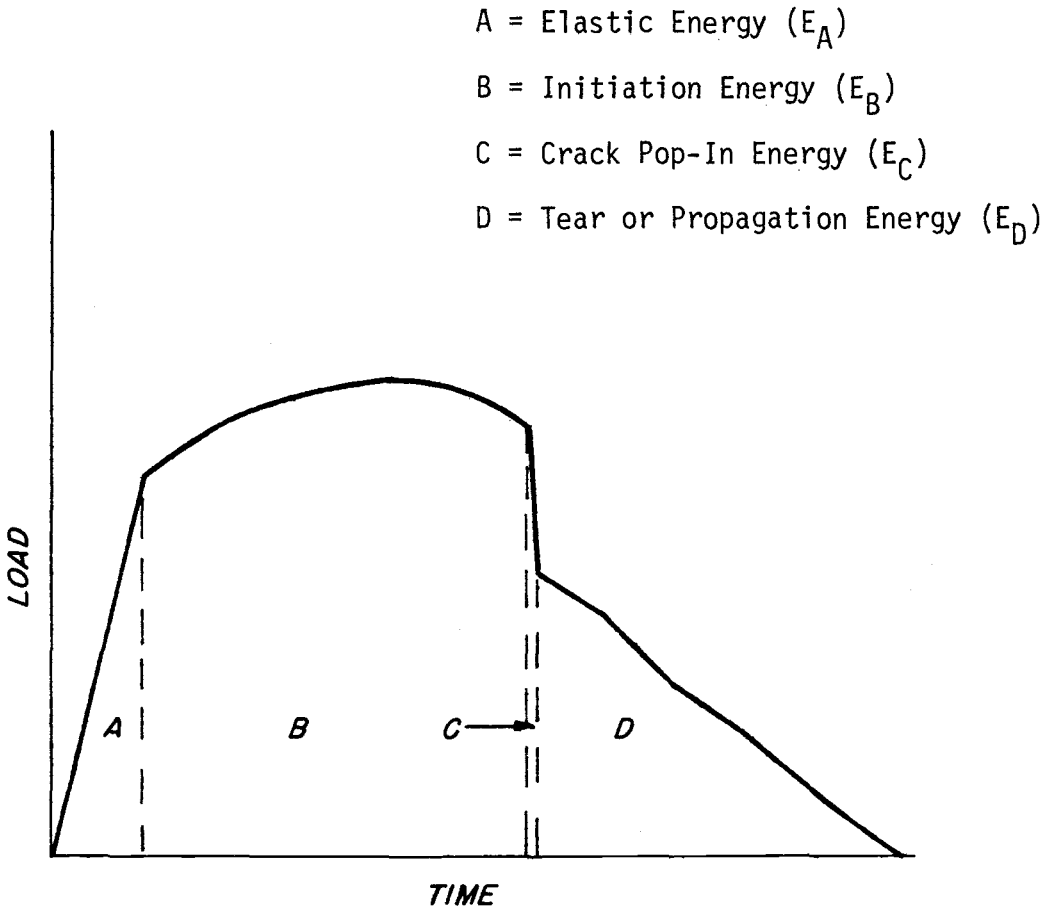

Figure 14. Typical load-time plot from an instrumented impact Charpy test of a ductile material. Energy areas representing the sequence of events during sample fracture are indicated by the letters.

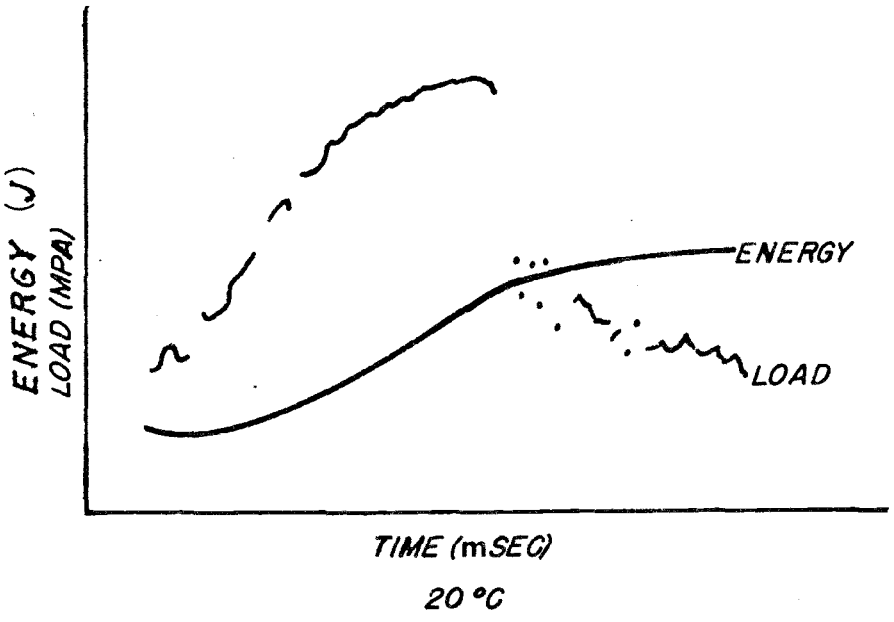

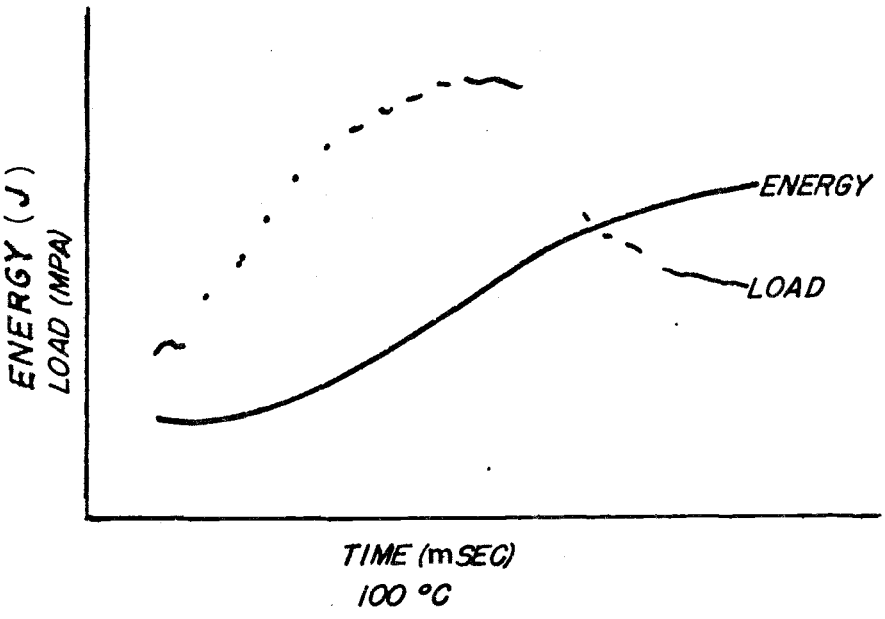

Figure 15. Typical load-time and energy-time plots at 20°C and 100°C for samples heat treated at 705°C for 2 hours and air cooled.

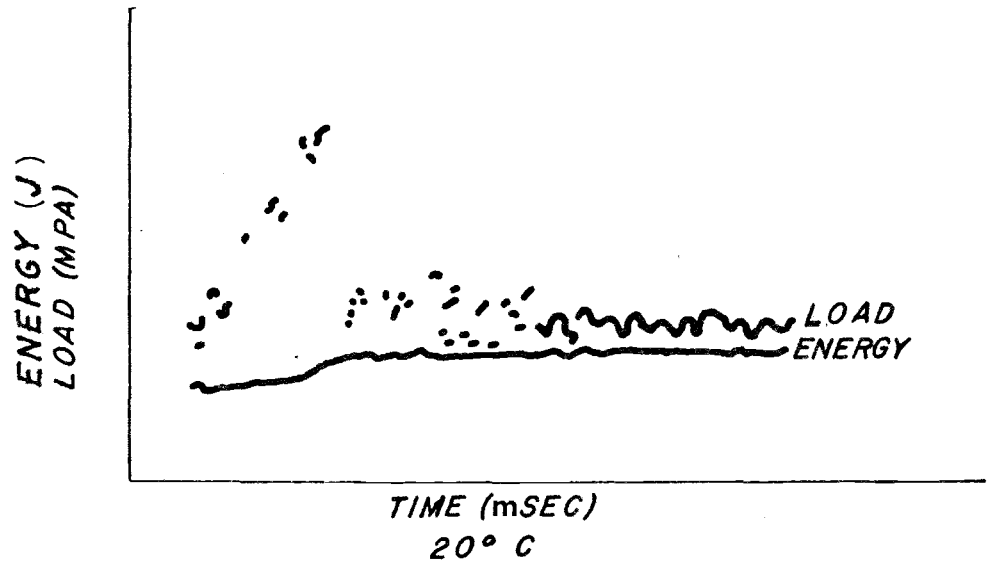

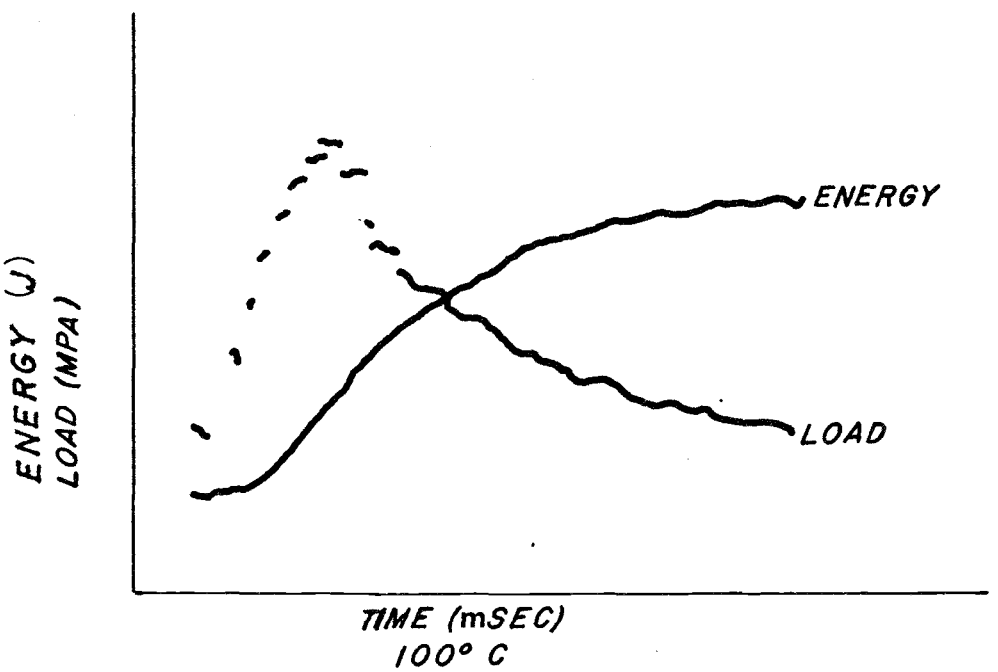

Figure 16. Typical load-time and energy-time plots at 20°C and 100°C for samples heated to 982°C for 1 hour and water quenched.

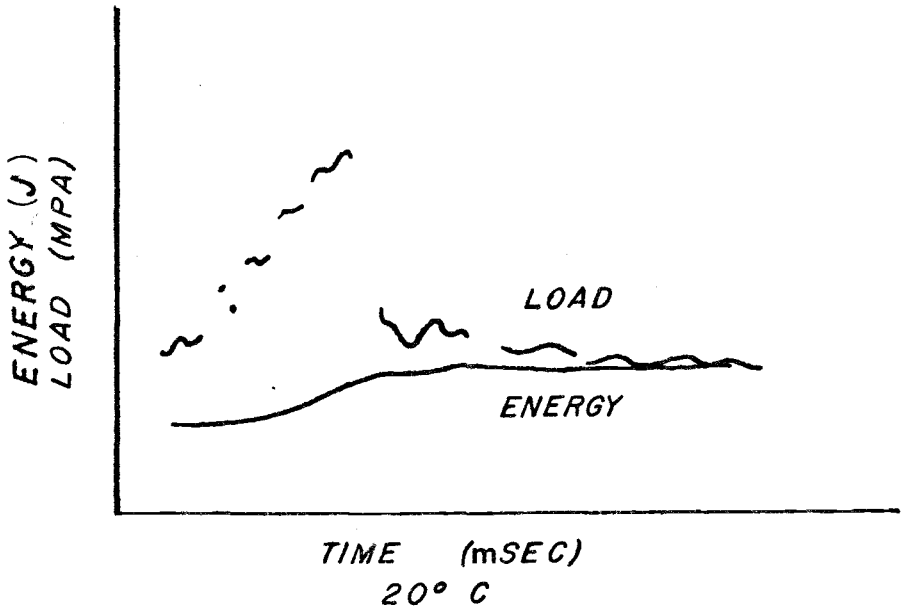

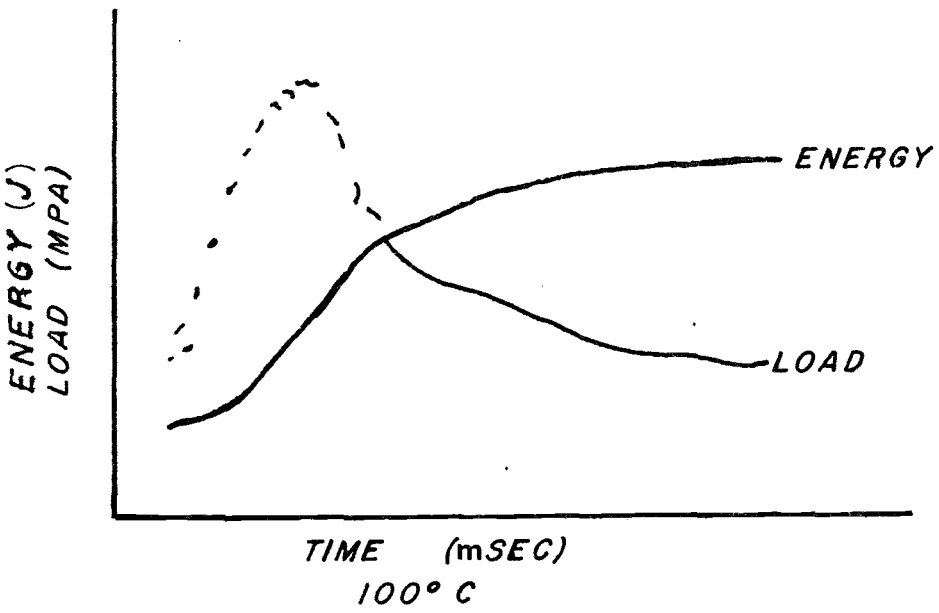

Figure 17. Typical load-time and energy-time plots at 20°C and 100°C for samples heated to 982°C for 1 hour and air cooled.

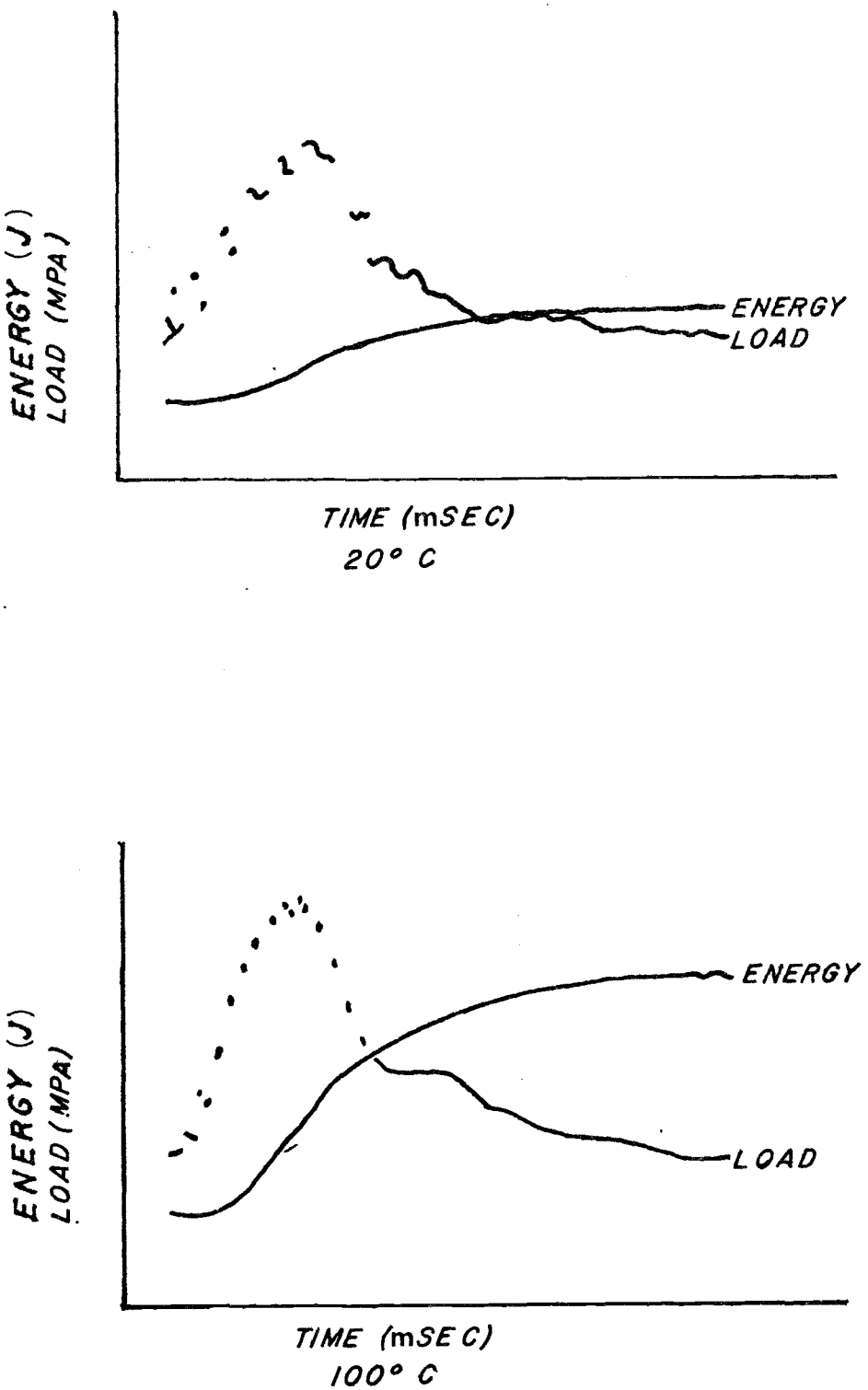

Figure 18. Typical load-time and energy-time plots at 20°C and 100°C for samples heated to 982°C for 1 hour and furnace cooled.

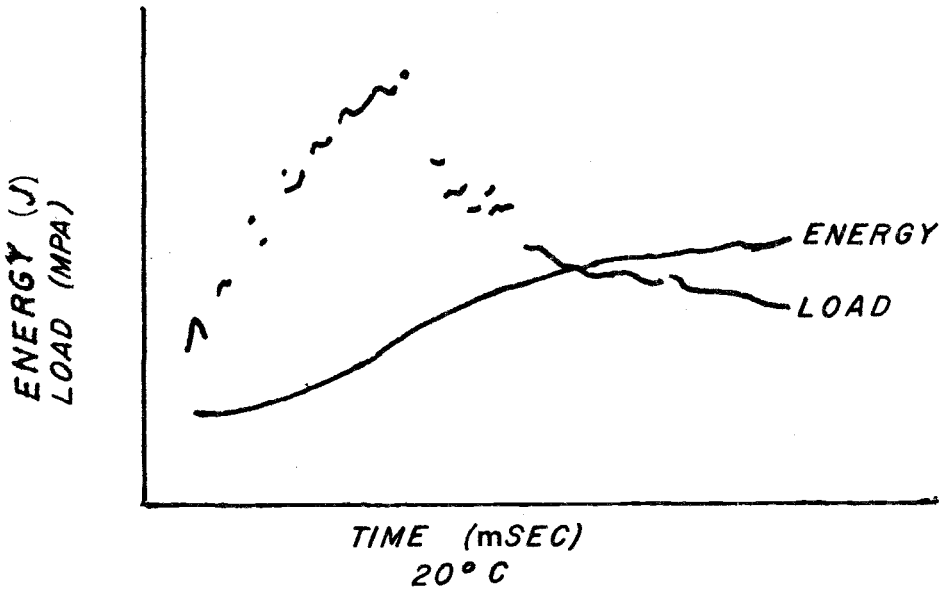

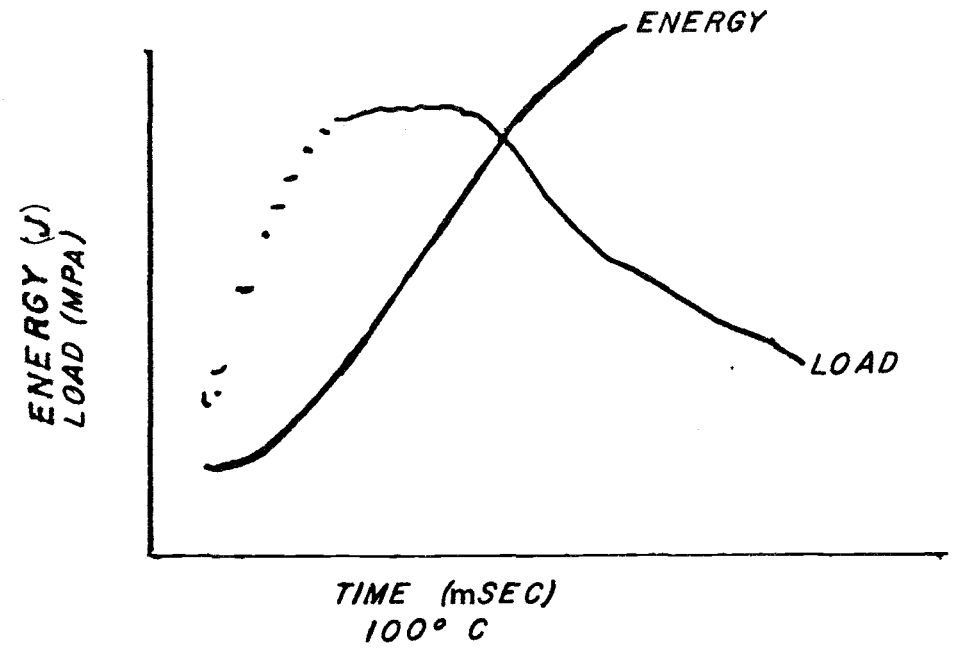

Figure 19. Typical load-time and energy-time plots at 20°C and 100°C for samples heated to 920°C for 1 hour and water quenched.

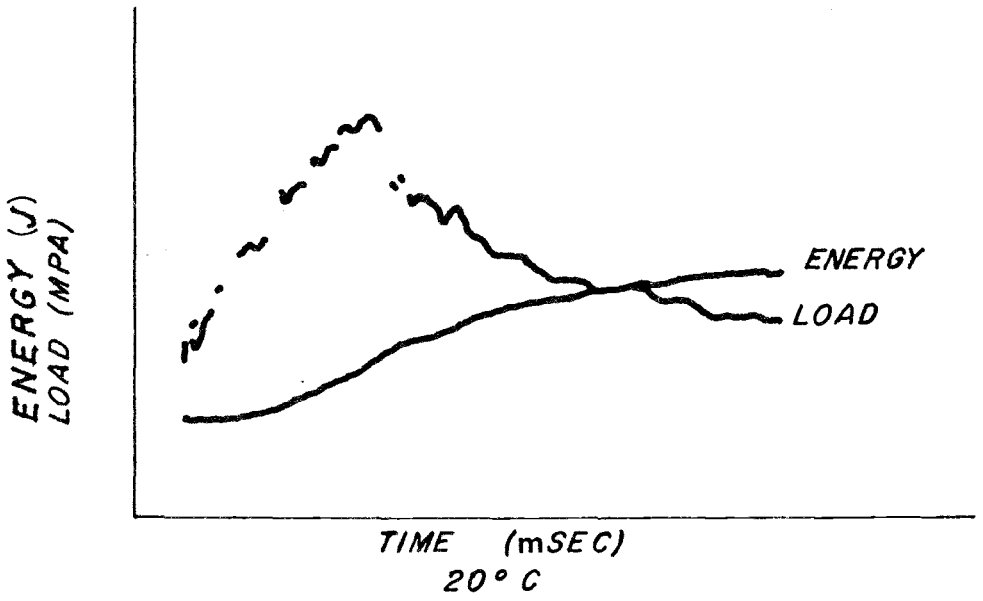

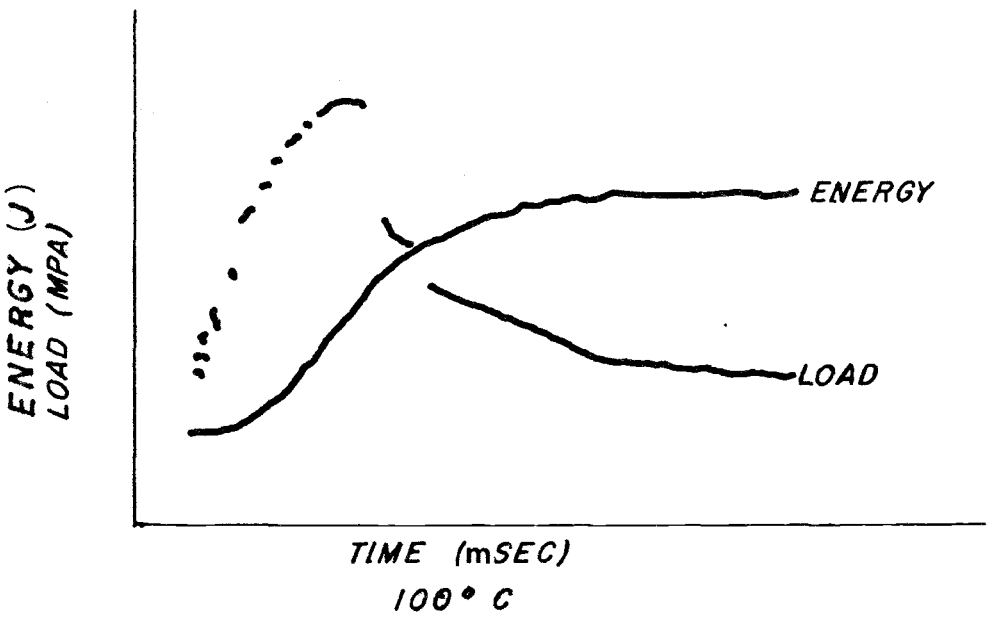

Figure 20. Typical load-time and energy-time plots at 20°C and 100°C for samples heated to 920°C for 1 hour and air cooled.

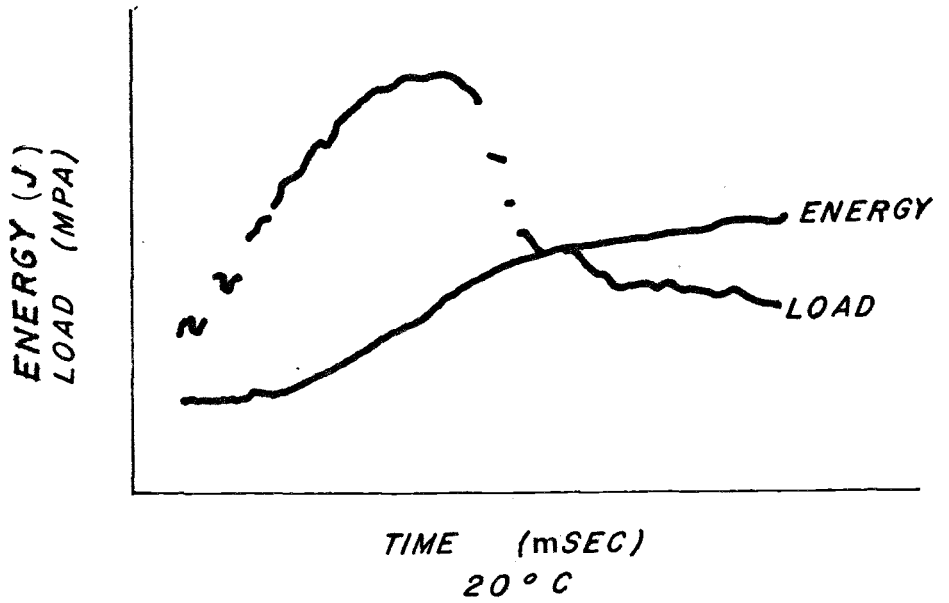

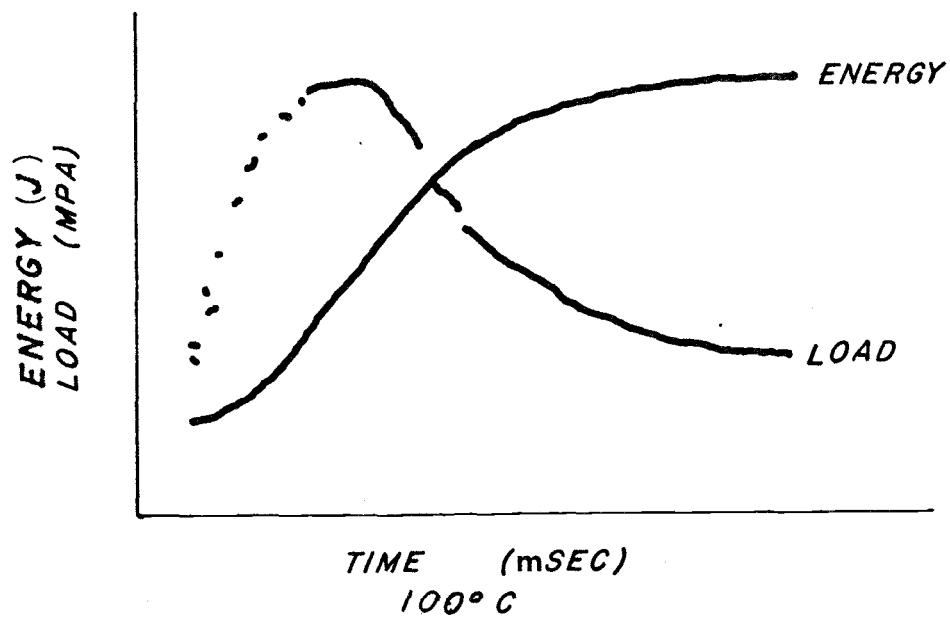

Figure 21. Typical load-time and energy-time plots at 20°C and 100°C for samples heated to 920°C for 1 hour and furnace cooled.

noted that for some of the curves the load-time trace did not return to the initial baseline, and the energy-time trace did not level out. This was due to the event time exceeding the horizontal display limit of the scope and required the curves to be graphically extrapolated. Examination of the load traces yields some interesting qualitative results. The initial rise portion of the 20°C trace in Figure 15 displays the sinusoidal nature of the tup signal, resulting from inertial effects, elastic energy, and reflected stress waves in the sample. Most of the curves have a somewhat fragmented initial rise due to the oscilloscope failing to completely record the signal during the rapid initial loading of the sample. Many of the curves exhibit an actual skip in the trace during crack pop-in, again as a result of the failure to graphically record a rapid event. In comparing the 20°C curves to the 100°C curves for all seven of the heat treated conditions, the increase in tear energy and the more complete line trace of the higher temperature tests are quite noticeable. This type of result not only represents more energy absorption but also indicates the overall fracture event is slower.

A complete compilation of the various energy divisions for both test temperatures and for all seven conditions of heat treatment is presented in Table III.

ROOM TEMPERATURE TEST RESULTS:

Because of the large number of energy values to consider and the complexity of the test event for each sample, a graphical analysis of the data is virtually mandatory. Figures 22 and 23 display the spectrum

TABLE III. IMPACT ENERGY RESULTS

Heat Treatment	Test Temp °C	Elastic Energy E_A(J)	Initiation Energy E_B(J)	Pop-In Energy E_C(J)	Tear Energy E_D(J)	Total Energy (J)	Tear % of Total Energy
	20	5.03	11.0	1.79	2.96	20.8	14.0
705°C for 2 hrs.	20	6.45	9.54	1.10	3.35	20.5	16.4
-Air Cool	20	4.80	10.9	0.945	4.66	21.3	21.9
	100	3.00	14.6	2.73	7.88	28.2	28.0
	100	4.09	15.7	2.73	7.13	29.7	24.0
	20	-	3.05	0.685	1.24	4.98	25.0
982°C for 1 hr.	20	-	3.09	0.617	0.359	4.07	8.8
-Water Quench	20	-	2.58	0.782	0.359	3.71	10.0
	100	2.41	8.68	3.90	16.8	31.8	52.9
	100	5.59	9.88	0.645	16.7	32.8	50.1
	20	-	4.56	0.519	2.64	7.71	34.3
982°C for 1 hr.	20	-	4.80	1.24	2.02	8.07	25.1
-Air Cool	20	-	5.19	0.656	3.02	8.88	34.0
	100	3.25	8.92	3.57	17.2	32.9	52.2
	100	2.48	10.9	1.90	14.2	29.5	48.2
	20	2.13	4.89	0.978	8.70	16.7	52.1
982°C for 1 hr.	20	2.16	3.90	0.945	4.46	11.5	38.9
-Furnace Cool	20	3.88	2.06	1.01	7.61	14.6	52.3
	100	2.55	4.66	-	12.1	19.4	62.7
	100	4.35	7.52	-	17.9	29.8	60.1
	20	5.06	6.52	1.24	10.8	23.6	45.6
920°C for 1 hr.	20	3.48	5.26	1.08	9.82	19.6	50.0
-Water Quench	20	2.13	4.70	0.656	4.64	12.1	38.2
	100	3.84	25.0	-	26.5	55.4	47.9
	100	3.06	19.4	-	25.0	47.4	52.7
	20	1.07	8.74	0.656	6.71	17.2	39.1
920°C for 1 hr.	20	2.22	4.70	0.880	10.7	18.5	57.7
-Air Cool	20	3.58	11.13	1.20	7.94	23.9	33.3
	100	2.09	15.0	1.50	11.1	29.7	37.4
	100	2.98	12.2	2.78	6.75	24.8	27.3
	20	4.75	8.32	0.782	5.42	19.3	28.1
920°C for 1 hr.	20	3.90	7.58	0.715	6.16	18.4	33.5
-Furnace Cool	20	4.09	5.17	1.34	6.29	16.9	37.2
	100	3.12	16.8	-	15.4	35.3	43.5
	100	3.77	11.2	3.06	9.45	27.5	34.4

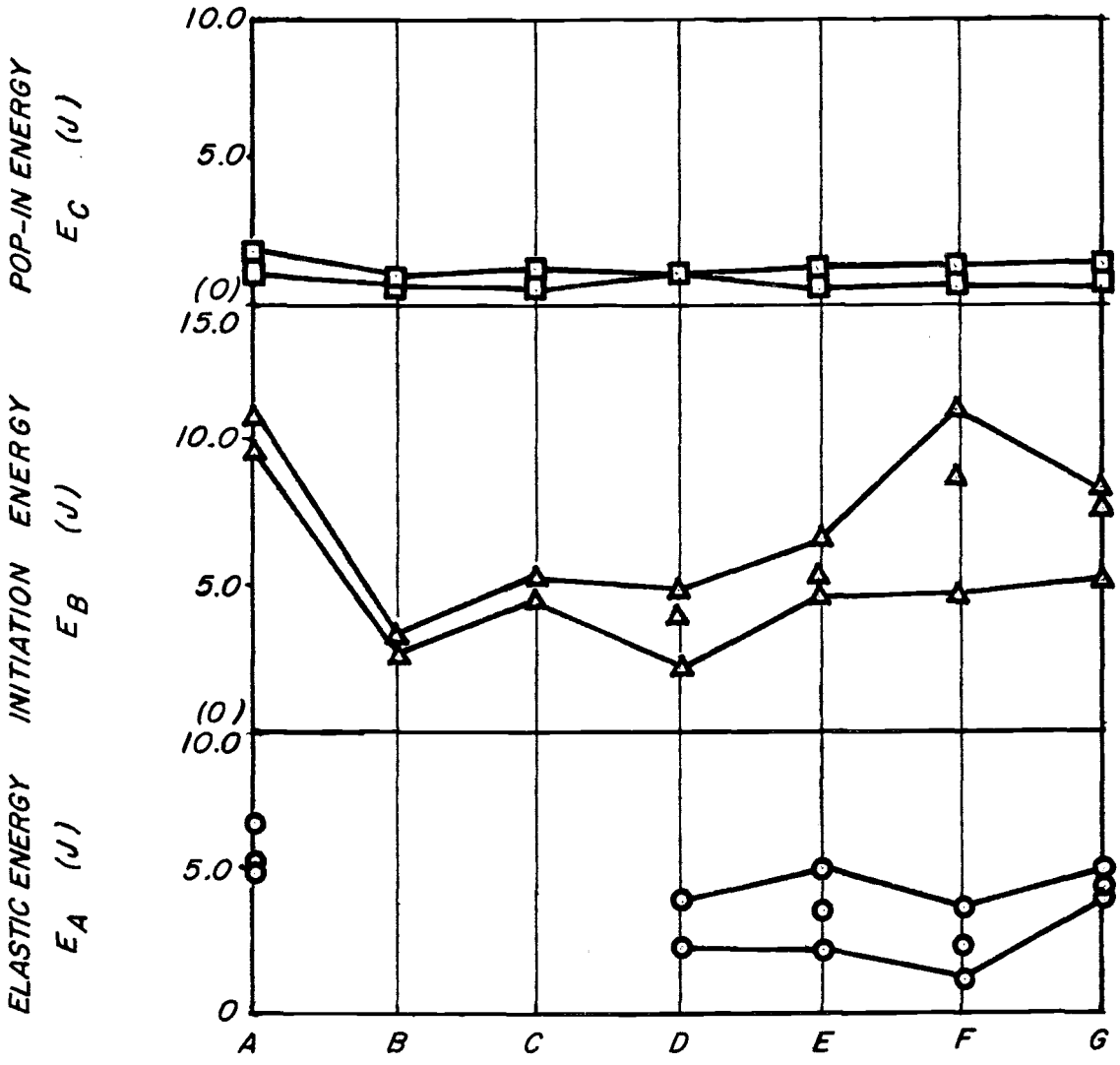

Figure 22. Elastic, initiation, and pop-in energies of impact samples tested at 20°C.
A = 705°C-2hrs/A.C., B = 982°C-1hr/W.Q.,
C = 982°C-1hr/A.C., D = 982°C-1hr/F.C.,
E = 920°C-1hr/W.Q., F = 920°C-1hr/A.C.,
G = 920°C-1hr/F.C.

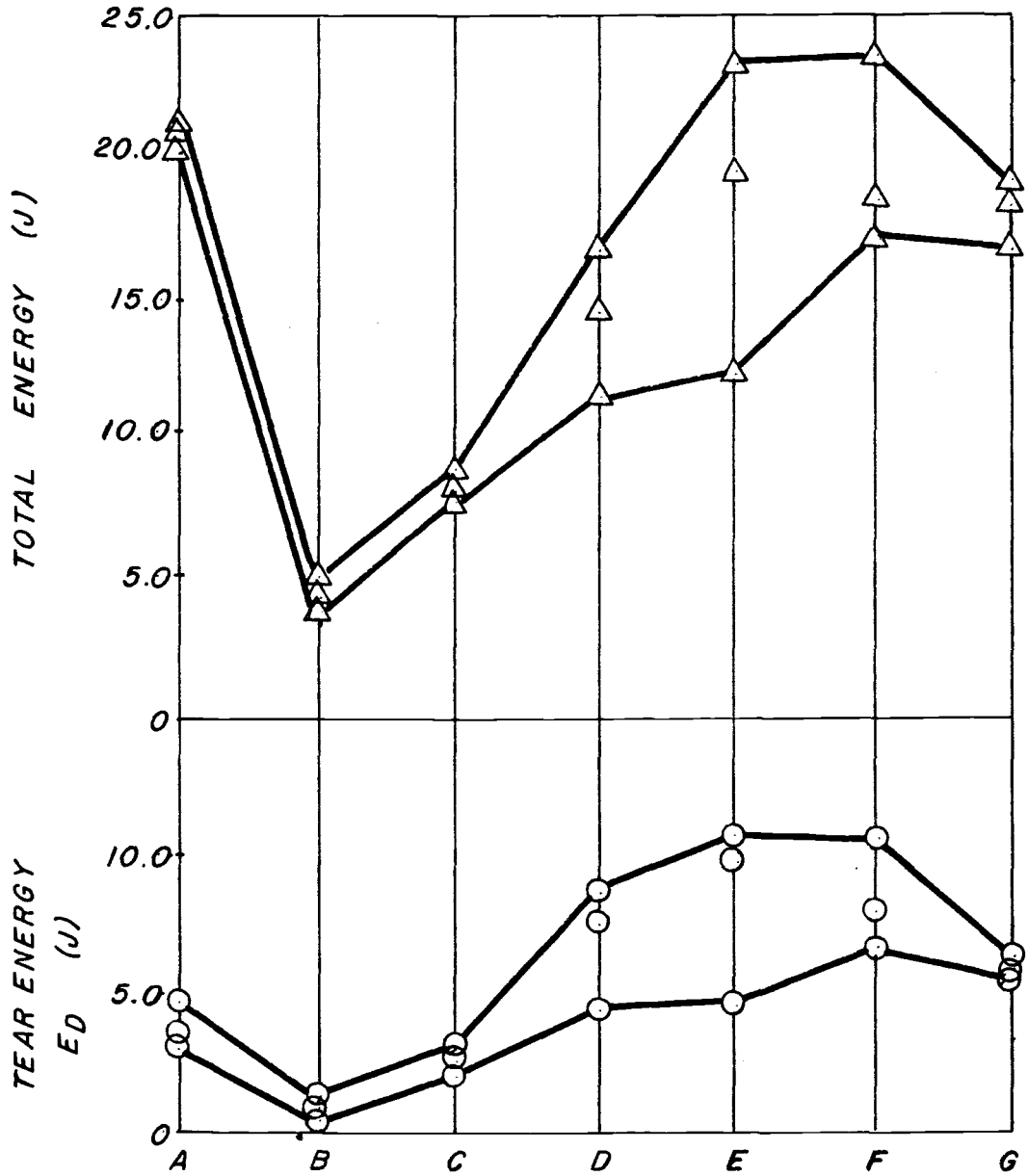

Figure 23. Tear energy and total energy of impact samples tested at 20°C. A = 705°C-2hr/A.C., B = 982°C-1hr/W.Q., C = 982°C-1hr/A.C., D = 982°C-1hr/F.C., E = 920°C-1hr/W.Q., F = 920°C-1hr/A.C., G = 920°C-1hr/F.C.

of energy values for each particular portion of the fracture sequence for the samples tested at 20°C. Although some data is missing for the elastic energy, this energy and the crack pop-in energy appear to be somewhat constant for the various heat treatments. This result is not surprising since both energies are basic material characteristics.

For the balance of the energies, the lowest energy condition is that representing the samples quenched from the beta phase field. The plot of the total energy in Figure 23 displays the low energy of the beta quenched structure most vividly. The general trend from the beta phase water quenched structure to beta phase slower cooled microstructures to the mixed phase microstructures at progressively slower quench rates, is a general increase in the particular energy type. These energy increases approach, and for the tear energy and total energy, surpass those of the annealed samples. The scatter of data for the mixed phase microstructures is significantly greater than that of either the annealed material or those samples cooled from the beta phase field. This data spread is an expected result and is likely due to the variation between samples of the relative amounts of the acicular or transformed structure and the equiaxed alpha structure. This microstructural variation was noted earlier in the characterization of heat treatment effects on microstructural phase constituents and percentages.

Figure 24 displays the variation in the percentage tear energy of the total energy with respect to the various heat treatments and cooling rates. It can be seen that the tear energy percentage increases gradually from the annealed state through the beta phase heat treatments to the mixed phase heat treatments. The maximum percentage is for the

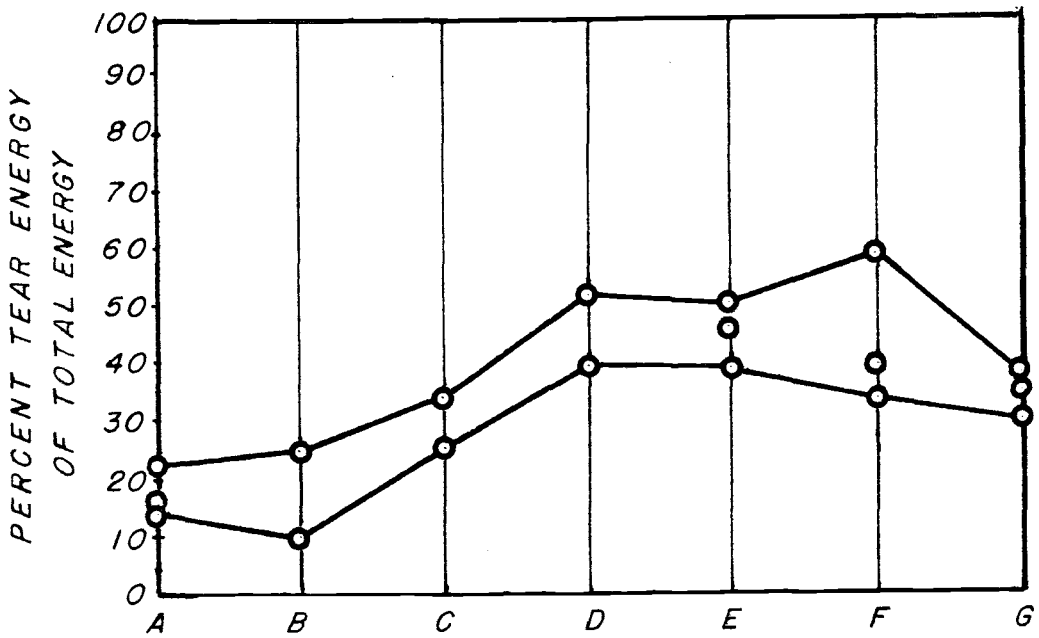

Figure 24. Percentage tear energy of total energy of impact samples tested at 20°C.
A = 705°C-2hrs/A.C., B = 982°C-1hr/W.Q.,
C = 982°C-1hr/A.C., D = 982°C-1hr/F.C.,
E = 920°C-1hr/W.Q., F = 920°C-1hr/A.C.,
G = 920°C-1hr/F.C.

mixed phase air cooled microstructure. However, both the furnace cooled beta phase heat treatment and all of the mixed phase heat treatments substantially increase the amount of the total energy required to propagate the initiated crack. From the standpoint of either heat treatment, the net effect appears to be an increase in tear energy absorption relative to the total energy absorbed by the samples. Heat treating in the two phase region followed by furnace cooling seems to be effective in returning the material to the original annealed state as evidenced by a decrease in the initiation, tear, and total energies, as well as a decrease in the percentage tear, over those values for the other heat treatments.

ELEVATED TEMPERATURE TEST RESULTS:

Figures 25 thru 28 are similar graphical representations of the various impact energies for the samples tested at 100°C. Again, both the elastic energy and crack pop-in energies appear to be fairly constant and independent of heat treatment. The remaining energy values are more sporadic with respect to heat treatment than in the 20°C test results. The mixed phase water quenched samples had the highest initiation, tear, and total energies of any of the samples tested at 100°C. The initiation energy is seen to decrease from the annealed state through the beta phase heat treatment at progressively slower cooling rates. Despite the dramatic increase in initiation energy with the water quenched mixed structure samples, the trend is again decreasing with slower quench rates. The tear energy is seen to increase significantly over that of the annealed samples for the other heat treatments.

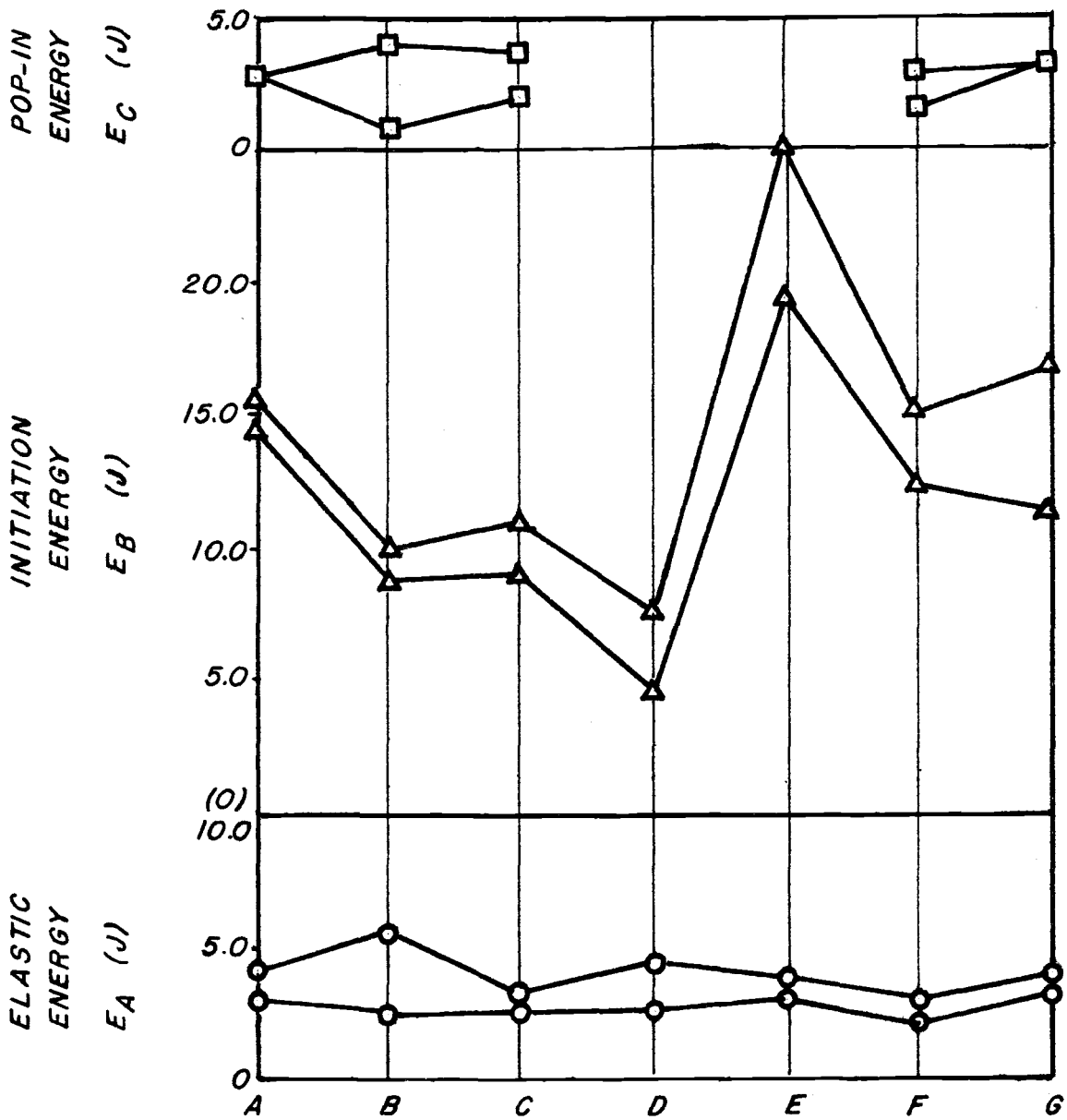

Figure 25. Elastic, initiation, and pop-in energies of impact samples tested at 100°C.
A = 705°C-2hrs/A.C., B = 982°C-1hr/W.Q.,
C = 982°C-1hr/A.C., D = 982°C-1hr/F.C.,
E = 920°C-1hr/W.Q., F = 920°C-1hr/A.C.,
G = 920°C-1hr/F.C.

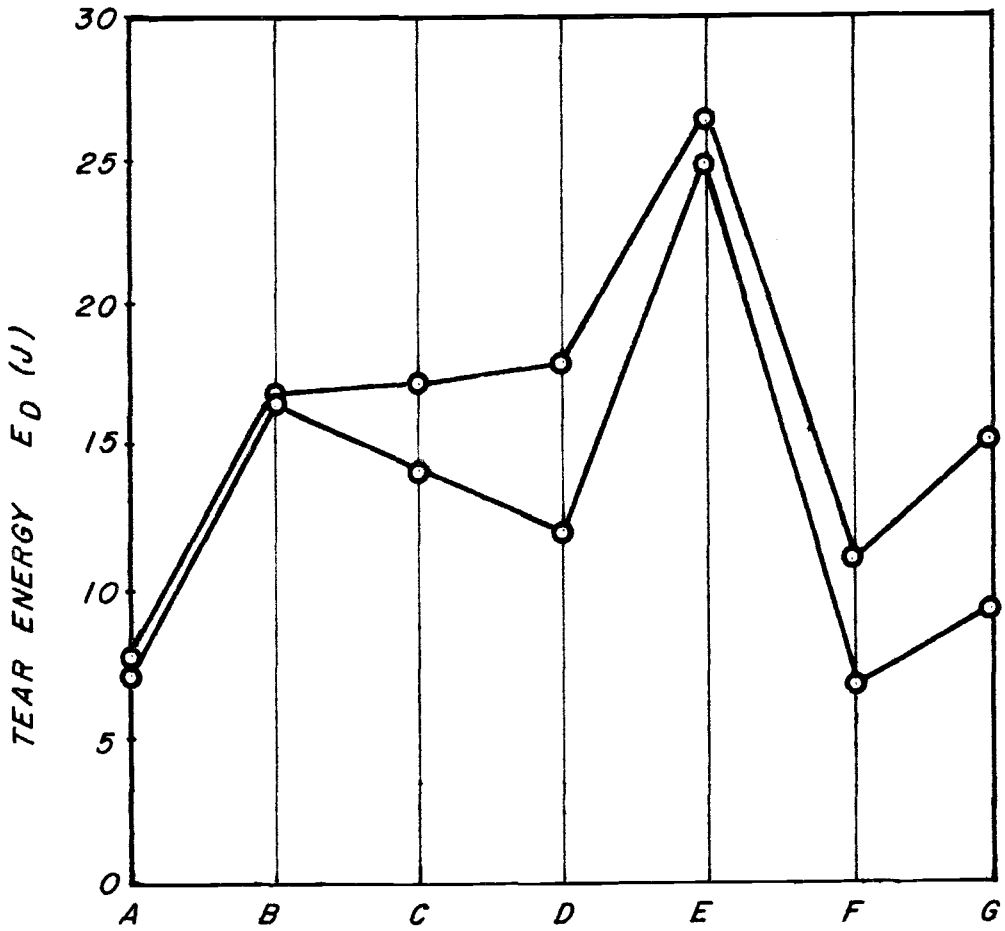

Figure 26. Tear energy of impact samples tested at 100°C. A = 705°C-2hrs/A.C. B = 982°C-1hr/W.Q., C = 982°C-1hr/A.C., D = 982°C-1hr/F.C., E = 920°C-1hr/W.Q., F = 920°C-1hr/A.C., G = 920°C-1hr/F.C.

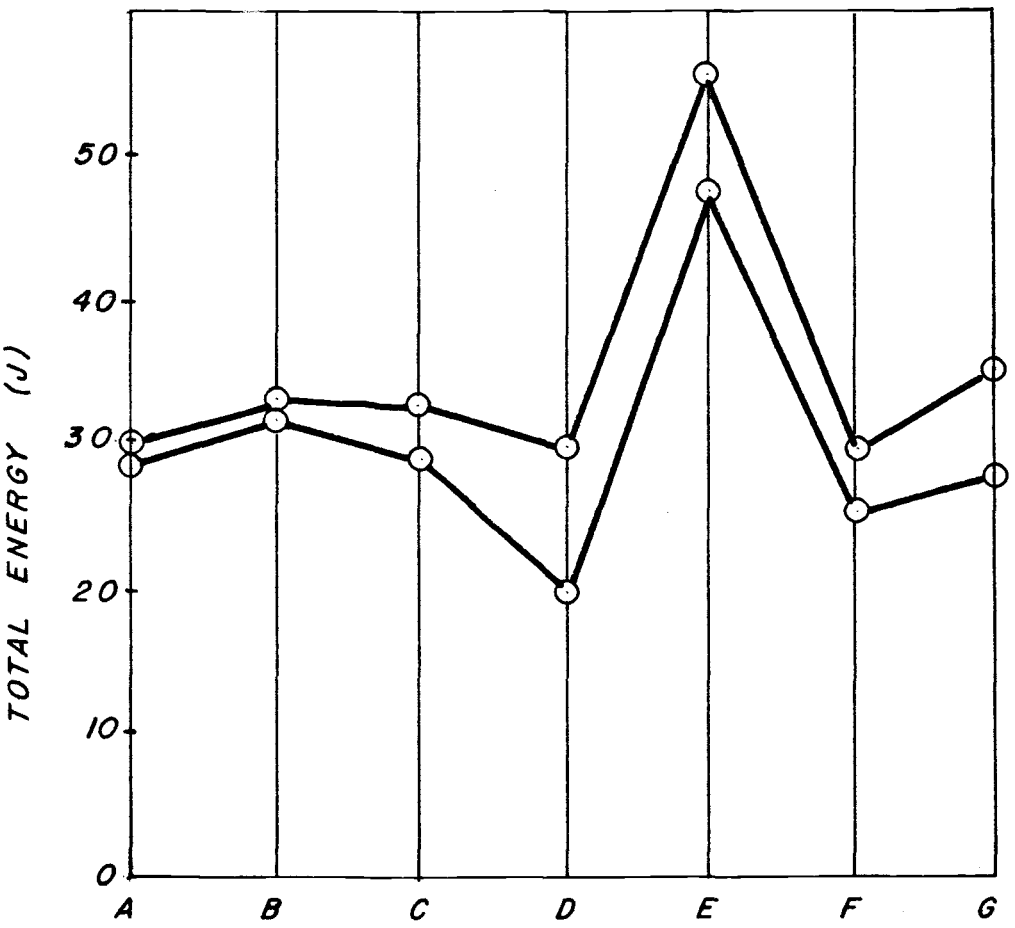

Figure 27. Total energy of impact samples tested at 100°C. A - 705°C-2hrs/A.C., B = 982°C-1hr/W.Q., C = 982°C-1hr/A.C., D = 982°C-1hr/F.C., E = 920°C-1hr/W.Q., F = 920°C-1hr/A.C., G = 920°C-1hr/F.C.

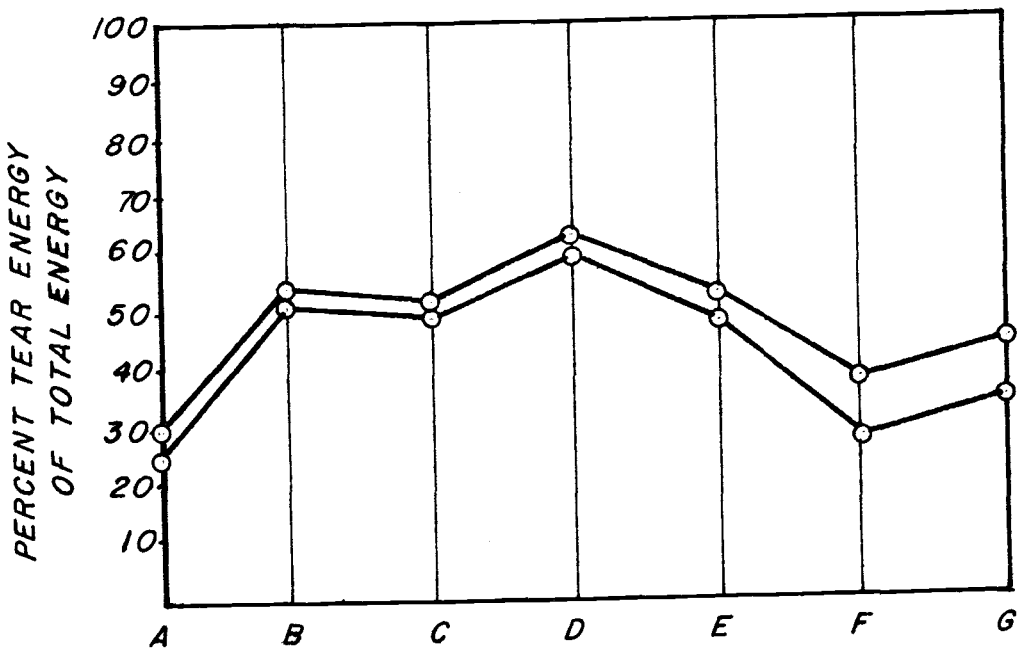

Figure 28. Percentage tear energy of the total energy of impact samples tested at 100°C.
A = 705°C-1hrs/A.C., B = 982°C-1hr/W.Q.,
C = 982°C-1hr/A.C., D = 982°C-1hr/F.C.,
E = 920°C-1hr/W.Q., F = 920°C-1hr/A.C.,
G = 920°C-1hr/F.C.

The samples heat treated in the beta phase field had somewhat constant tear energies with respect to cooling rate whereas the mixed phase samples do not show any trends except for the higher tear energy of the water quenched samples. The total energy values seem to be somewhat constant to slightly increasing with regard to heat treatment, again with the exception of the mixed phase water quenched samples.

The amount of data scatter in the tear energy percentages for the higher temperature test results is significantly less than that of the samples tested at 20°C. This is especially true of the mixed phase samples, where variations in the amount of phase constituents did not seem to drastically affect absorbed energy values. The general trend of the variation in tear energy percentage with heat treatment is similar to that observed in the samples tested at 20°C. The samples heated in the beta phase region, however, seem to display somewhat greater tear percentages for the 100°C tests than for the 20°C tests.

EXAMINATION OF TEMPERATURE EFFECTS:

To determine the effect of temperature on the various energy increments and the total energy, a graphical comparison was made. Figures 29 thru 31 depict the various energies at 20°C and 100°C for all seven of the heat treated conditions. For most of the heat treatments, the most significant amounts of increases in energy values with temperature seemed to be in the tear energy and total energy. The greatest increases in total energy occurred with the water quenched structures, either of mixed phase or quenched from the beta phase field, and those samples air cooled from the beta region. The same general trend can also be applied

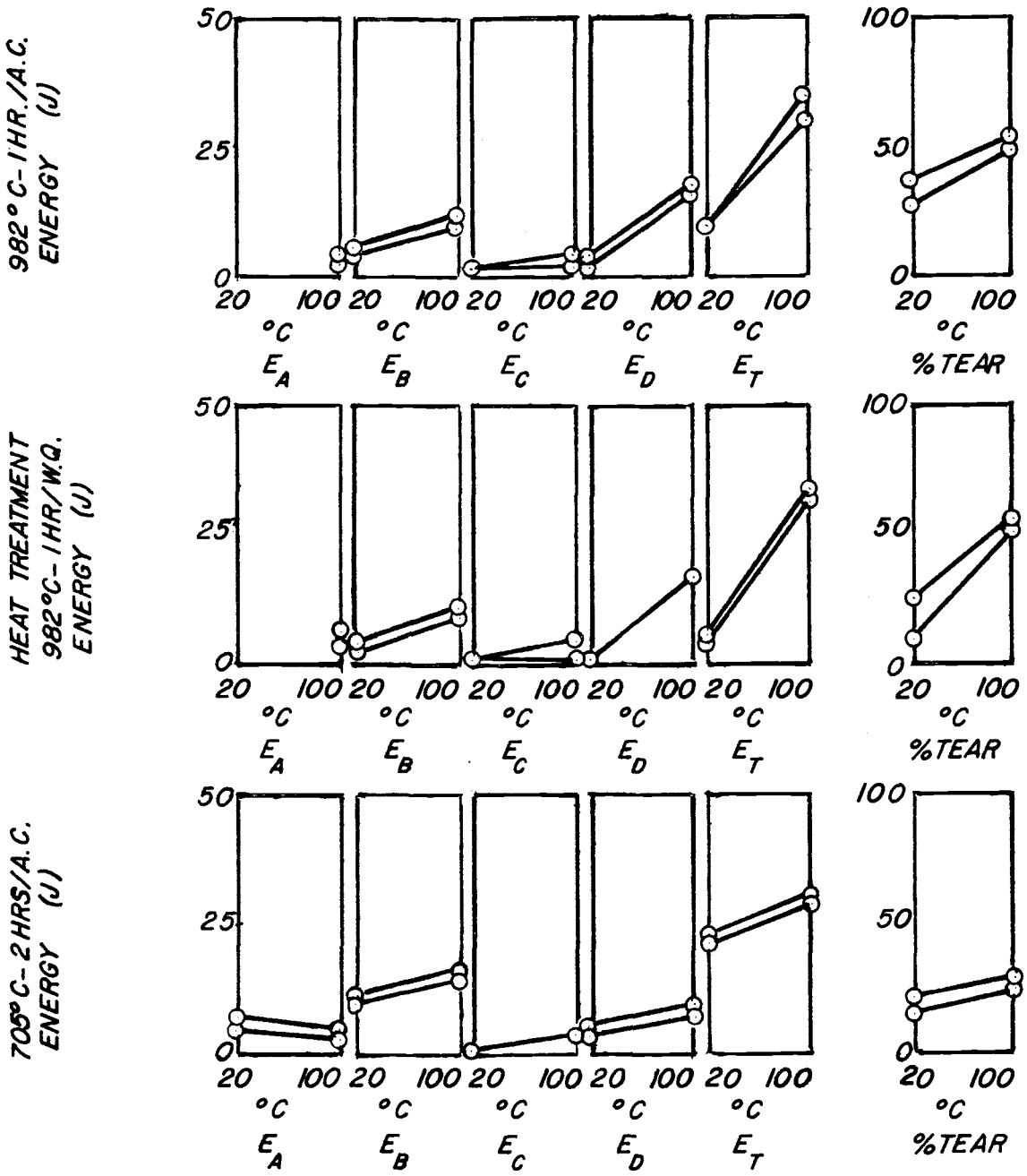

Figure 29. The effect of test temperature on the various energies for the following heat treatments: 705°C-2hrs/A.C., 982°C-1hr/W.Q., 982°C-1hr/A.C.

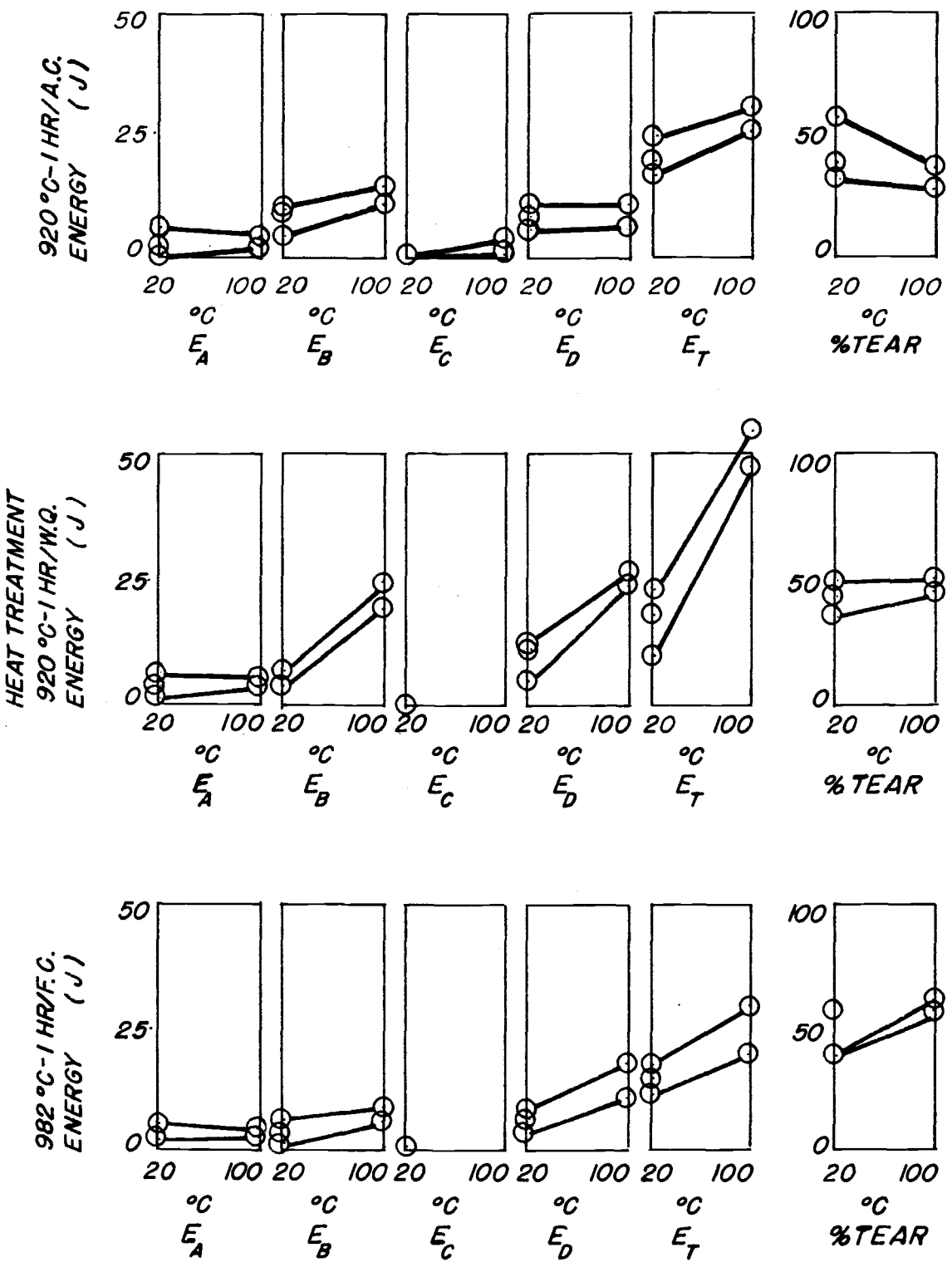

Figure 30. The effect of test temperature on the various test energies for the following heat treatments: 982°C-1hr/F.C., 920°C-1hr/W.Q., 920°C-1hr/A.C.

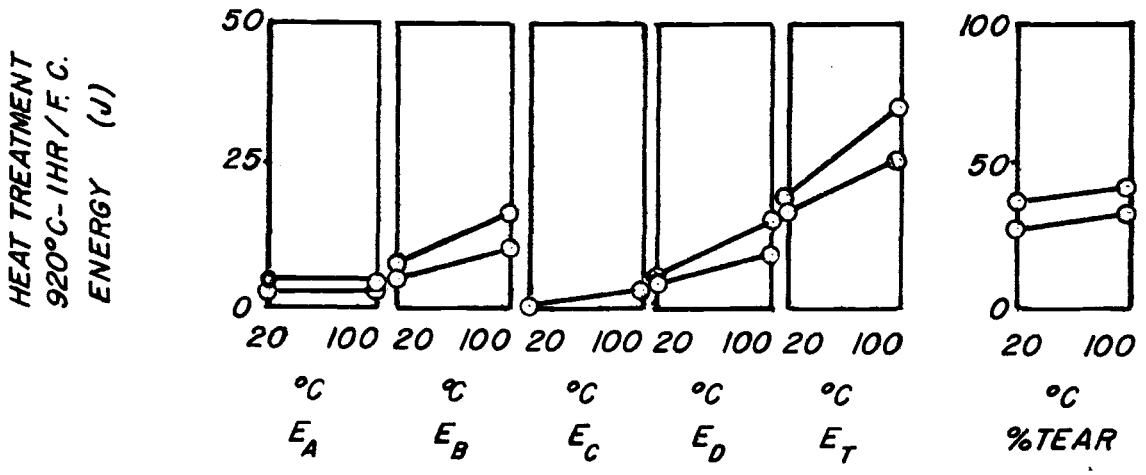

Figure 31. The effect of test temperature on the various impact energies for the samples heat treated at 920°C-1hr/F.C.

to the tear energies for these heat treatments. The initiation energy seemed to increase with temperature to some extent in all seven heat treatments. However, the elastic energy and crack pop-in energy were, in general, constant. The largest temperature transitions for the percent tear energy values seemed to occur in those samples heat treated in the beta phase region, with much smaller, or even negative transitions occurring in the other heat treated conditions. From the above observations, it is evident that the acicular type structure exhibits a significant brittle to ductile transition in the temperature range of 20°C to 100°C. This transition seems to occur whether the acicular phase morphology is the principle constituent or just a partial component of the microstructure. The transition to higher impact energies definitely occurs above 20°C but may extend to temperatures higher than 100°C before the energy-temperature curve decreases in slope.

Although the water quenched mixed phase structure displayed the highest energy observed in this study when tested at 100°C, 55 joules, the greatest increase in energy over that of the 20°C test samples occurred in the samples water quenched from the beta phase field. The increase in total energy in this instance was almost sevenfold, whereas in the former case, it was only three to four times greater. The substantial increase in toughness with temperature for those specimens water quenched from the beta phase field represents an extreme sensitivity to testing temperature.

For those samples exhibiting the greatest total energy values, unsuccessful attempts were made to measure a lateral expansion on the end of the specimens. The variation in machining tolerance probably

masked the detection of any expansion that might have occurred.

SUMMARY OF MECHANICAL TEST RESULTS:

In examining all of the test results, a consistent trend seems to develop with regard to heat treatment. For the ultimate and yield strengths, water quenching from the beta phase field increases the strength values over that of the annealed material. However, with all of the additional heat treatments, both yield and ultimate strengths gradually decrease. This same trend is apparent in the hardness values. In contrast, both elongation and reduction of area drop to their lowest values with the beta phase heat treatment and then return to the approximate ductility of the annealed material for all three mixed phase heat treatments.

The results of the 20°C impact tests generally exhibit a decrease in the initiation, tear and total energies for the water quench beta phase heat treatment, with the energies subsequently increasing for each additional heat treatment. This same trend is not so pronounced in the samples tested at 100°C however. For both testing temperatures, the elastic energies and pop-in energies appear to remain somewhat constant.

The inverse direction of property shift between the tensile and the impact test results seems to be consistent with an increase in material toughness with each subsequent heat treatment. For the samples water quenched from the beta phase field, the strength values were higher than the annealed material, but both the ductility and impact energies were lower. As the strength values decreased in magnitude for the remaining heat treatments, the toughness tended to increase along with the

ductility. The one anomalous result is the low elongation and reduction of area values exhibited by all three heat treatments in the beta phase region. This limited sample ductility seems to be inconsistent with the microstructure reverting back to the annealed structure morphology and the general trends exhibited by the other mechanical properties.

The increase in spread between the yield and ultimate strengths for the mixed phase microstructures does not seem to correlate with any of the impact results, or with the ductility values of these particular tests. The greater work hardening displayed by these samples is not indicated by any specific toughness trend other than the previously noted general increase in toughness with the various heat treatments.

VI. FRACTURE SURFACE EXAMINATION

OPTICAL FRACTOGRAPHY:

The fracture surfaces from all of the tensile test specimens and impact specimens were examined with the unaided eye and with the aid of a stereomicroscope, at magnifications up to 70 diameters. The following observations were made.

The one annealed tensile test sample and all of the tensile samples with mixed phase microstructures exhibited normal characteristics of ductile fracture in tension. All of these specimens displayed a cup-cone type fracture surface with extensive necking in the region of final failure. Surface deformation or mottling was present on all of the samples for most of the reduced section. The annealed sample fracture surface was finely textured with no evidence of secondary cracking. The mixed phase samples exhibited a somewhat coarser texture than that of the annealed bar, but were otherwise quite similar.

Those samples representing the beta phase heat treatments had a significantly coarser fracture topography. Specimens from all three cooling rates displayed large, smooth, planar facets and protrusions from the principle fracture plane. Examination of these fracture surfaces at higher magnification revealed significant amounts of secondary cracking at low angles to the specimen axis. The general orientation of the planar surfaces and the secondary cracking was quite indicative of the acicular nature of the microstructures. The water quenched samples exhibited the most pronounced planar features with one of the

samples failing along the 45° shear plane with little texture visible on the facet surface. All of the samples cooled from the beta phase region exhibited minimal necking and deformation in the vicinity of the fracture, as confirmed by their low elongation and reduction of area values.

Similar features to those observed in the tensile fractures were noted for the impact fracture surfaces. Figure 32 shows representative fractures for all of the heat treatment and cooling rate combinations for the samples tested at 20°C and 100°C. Only minor differences can be observed between the two testing temperatures. As noted in the tensile specimens, the fracture topography and surface texture of the annealed bars and those with mixed phase microstructures exhibit similar characteristics. Some coarsening of the annealed fracture surfaces is noted in the samples heat treated at 920°C, but the general features of the fracture surfaces for both of these heat treatments are basically of a fine textured nature. One interesting observation noted in the mixed phase samples is the appearance of dark specs uniformly distributed across the fracture surfaces when examined with the unaided eye. This feature is easily discernable in the 920°C-FC sample tests at 20°C in Figure 32. At higher magnifications, these dark features appear to be deep tears or gouges in the fracture surface with rough sides and bottoms, unlike what one would expect for voids resulting from gas entrapment. These tear pits are generally circular and were most pronounced in those samples tested at 20°C.

The samples cooled from the beta phase field had the same general coarse fracture topography noted in the tensile specimens. Numerous planar facets were present in samples from all three cooling rates. No

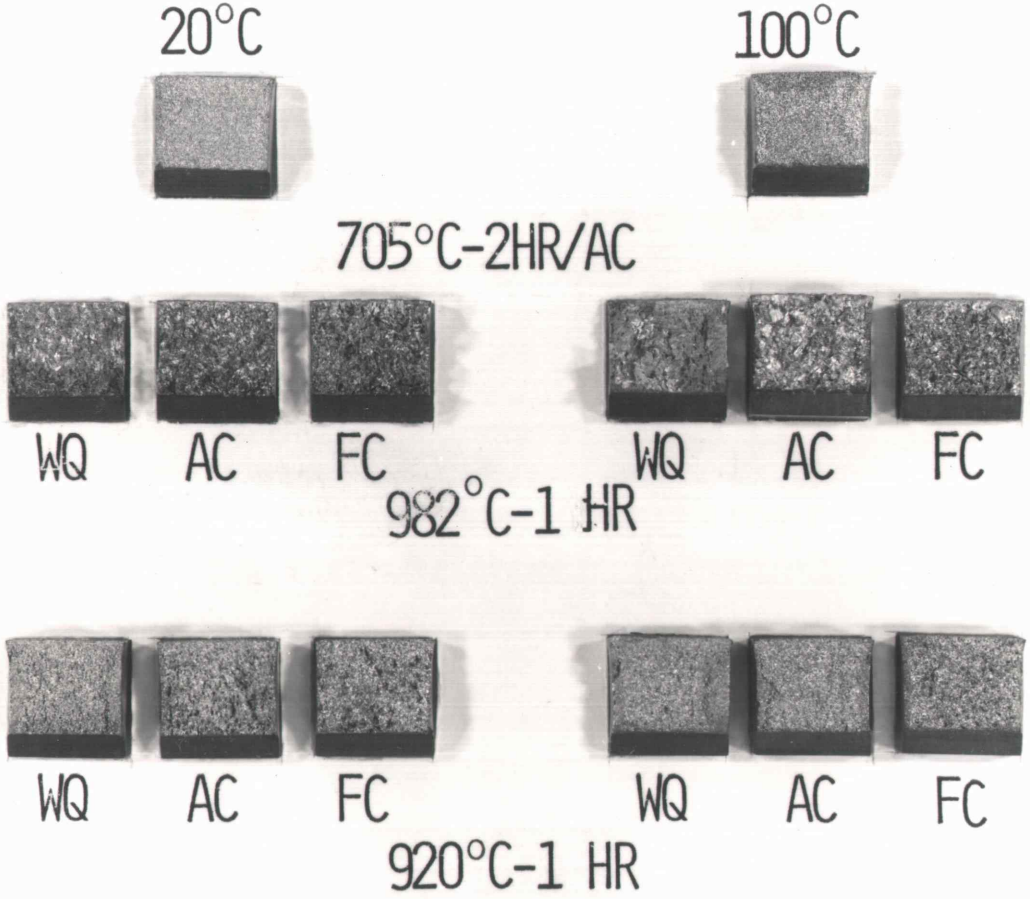

Figure 32. Representative impact fracture surfaces for all of the various microstructures, tested at 20°C and 100°C.

significant change in fracture surface appearance was noted for those samples tested at 100°C. Few of the samples from this heat treatment exhibited shear fracture that exceeded 10% of the fracture surface, with most of the samples exhibiting less than 1% shear. The designation of shear fracture was by the extension of the fracture above the principle fracture plane on either side perpendicular to the notch. In all cases, the texture of the shear region was identical to that of the principle fracture surface.

The development of shear lips or shear fracture was somewhat more pronounced in those samples having a mixed phase microstructure. Although the amount of shear fracture was generally 10% or less of the total fracture surface in the samples tested at 20°C, the significantly tougher samples tested at 100°C displayed somewhat more shear area. The representative sample water quenched from the alpha-beta region shown in Figure 32 is seen to have from 20 to 25% shear fracture. This was the highest percentage shear noted in any of the samples, and was likely related to the higher energy absorption of the water quenched samples when tested at elevated temperature. None of the annealed samples for either test temperature exhibited shear fracture greater than 1% of the total fracture area.

SCANNING ELECTRON FRACTOGRAPHY:

Scanning electron microscope examination of the tensile and impact fracture surfaces of samples representing all of the heat treatments yielded some surprising results. Almost all of the fracture features observed were quite coarse and few required magnifications greater than

400X to completely resolve. In most cases, the observed features were complementary and consistent with those made optically.

The fractograph shown in Figure 33 is representative of the typical fracture topography of the annealed material when fractured in tension. The predominant feature is that of large elongated dimples and tear ridges. With higher magnification, the base of the dimples contained some fine line patterns, but were generally featureless. A few localized areas were observed where the dimple network was somewhat more shallow and considerably finer in size. This local topographic difference may be the result of fracture of the beta phase, while the predominant dimple and tear features are attributed to the alpha phase.

The fracture surfaces of the tensile bars quenched in water from the beta phase field were radically different from those of the annealed material. Shown in Figure 34 are the most commonly noted features of these fractures. The flat facets shown in this figure were present over the entire fracture surface and exhibited a significant amount of between facet secondary cracking. Higher magnification of these facets revealed a subtle tear pattern that was quite indicative of the acicular nature of the microstructure, as shown in Figure 35. The similarity of these features to that of the microstructural morphology is further noted in the coarse raised ridge pattern outlining the areas of subtle ridges. This raised region may represent the separation between adjacent Widmanstätten plates. Its overall size, however, is too small to be representative of the beta grain size of the material. The fracture between these facets consisted of a shallow dimple network. These dimples were generally circular in shape and much finer than those observed

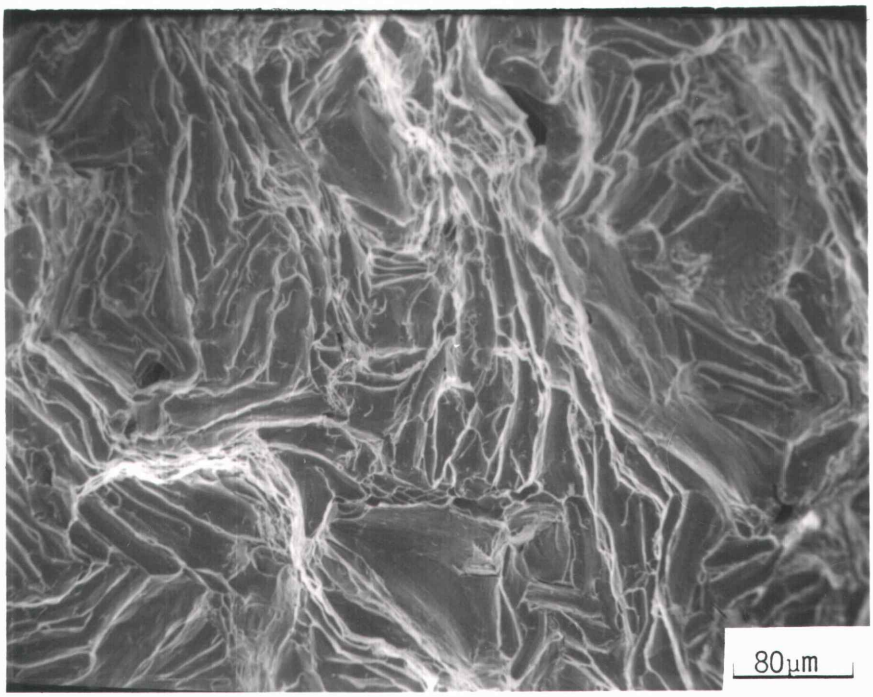

Figure 33. Typical coarse dimpled fracture surface of annealed material, 200X.

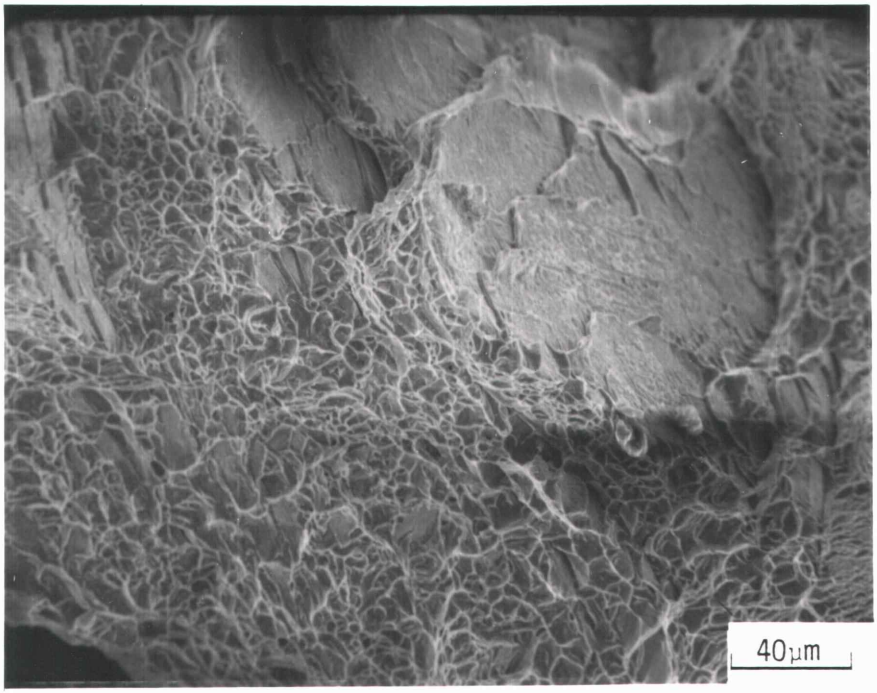

Figure 34. Fracture surface from tensile bar water quenched from the beta phase field. Note fine, uniform dimple structure and large facets, 400X.

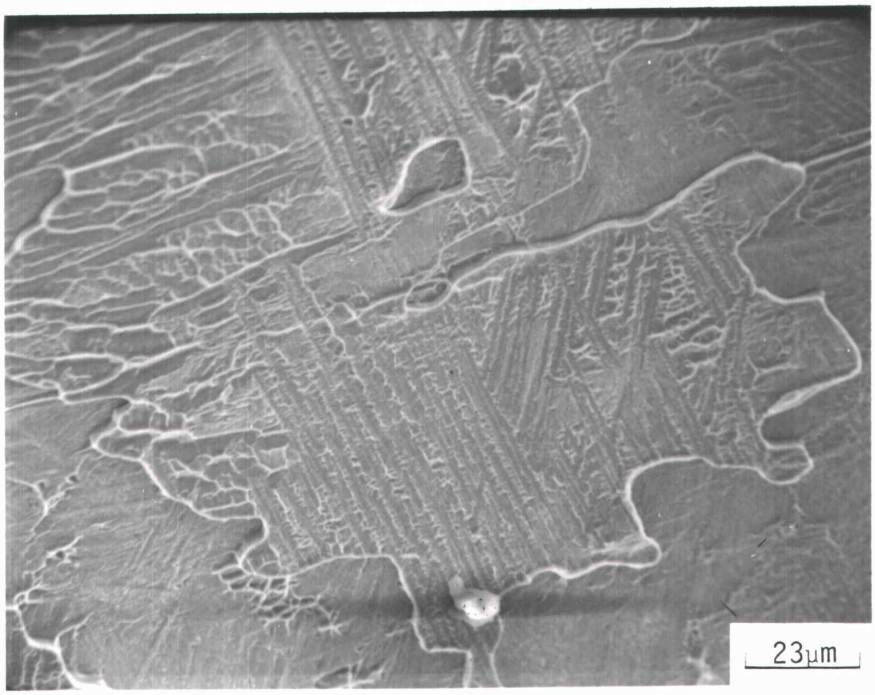

Figure 35. Higher magnification view of facets shown in Fig. 34 reveal subtle and directional tear patterns, 700X.

in the annealed tensile fractures, although they did seem to resemble the more localized dimples seen in the latter samples attributed to the beta phase.

Those samples air cooled from the beta region displayed the same general features as those of the water quenched tensile fractures. In this instance, however, the raised tear patterns on the facets were smaller and there were generally more tear ridges and shallow dimples. The fine acicular pattern seen in the water quenched fractures was also present on the facets in these fractures.

The beta phase furnace cooled tensile samples displayed a fracture topography similar to that of the annealed material. Figure 36 shows the general elongated nature of the coarse dimples similar to those in Figure 33. In these samples, however, the degree of orientation is greater and an apparent boundary between adjacent groups of aligned needles is quite visible. Figure 37 is a higher magnification view of the boundary area and adjacent material. An extensive region of shallow circular dimples is seen to predominate not only the boundary region but also the area between some of the aligned needles. The fine texture observed on three of the facets visible in Figure 37 could not be attributed to any microstructural feature.

All of the tensile fractures from the mixed phase microstructures were essentially identical. Figure 38 from a mixed phase water quenched sample is a typical representation of the coarse dimple pattern observed in the annealed samples broken in tension. It is informative to note, however, that there is a significantly larger portion of the fracture that displays the fine and shallow circular dimples than in

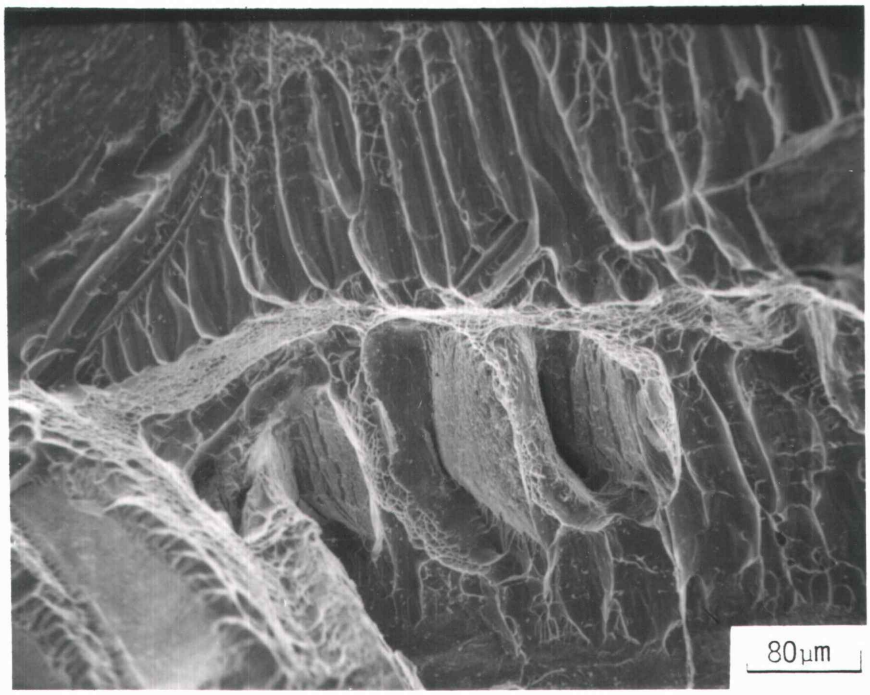

Figure 36. Coarse elongated dimple network in tensile bar sample furnace cooled from the beta phase field, 200X.

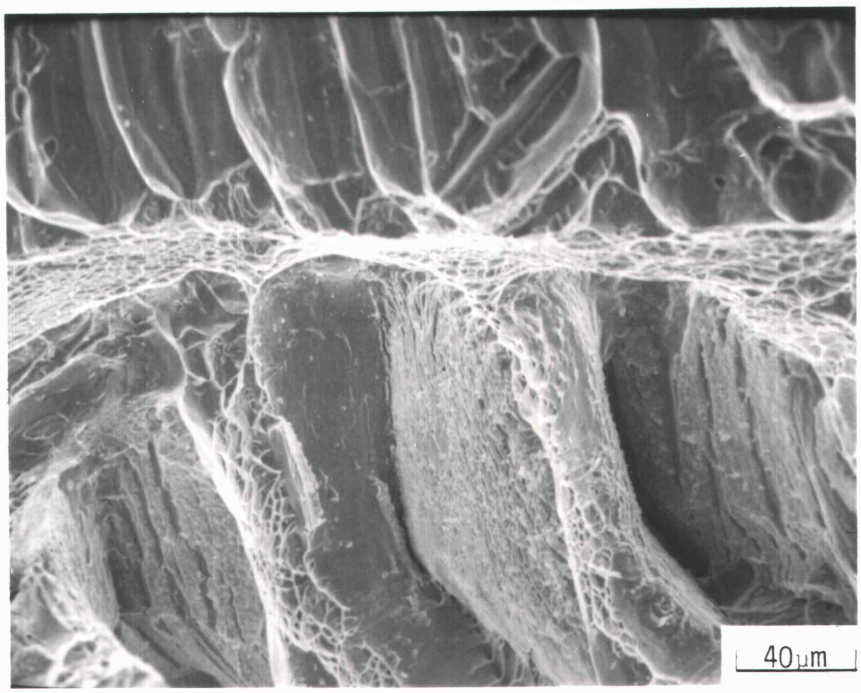

Figure 37. Higher magnification view of ridge between aligned dimples in Fig. 36 reveals finer dimple network, 400X.

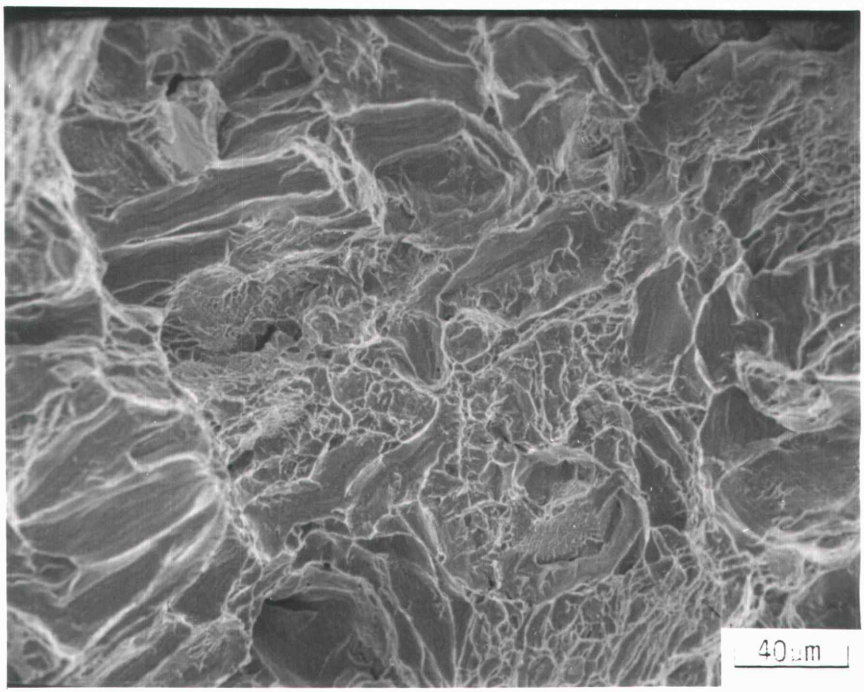

Figure 38. Tensile fracture surface of sample water quenched from the two phase field. The shallow dimple networks are a significant portion of the total fracture features, 400X.

the annealed samples. The general shape and population of these shallow dimpled regions is consistent with that of the regions of acicular alpha phase. For this particular magnification, the general size of these regions is close to that of the transformed areas of the microstructure.

The fractographic features of the impact samples were in general consistent with that of the tensile bars. Since the predominant features are identical to those of the tensile fractures, no characterizing fractographs will be presented here. The distinctive feature of the deep tear pits noted optically in some of the mixed phase samples was confirmed in the SEM examination of these particular fracture surfaces. The inside wall of these tear pits contained both smooth surfaces and tear ridges, identical in nature to the balance of the fracture surface.

A particularly interesting observation can be made with regard to the impact fractures when comparing those fracture surfaces of the samples tested at 20°C to those tested at 100°C. Figure 39 was taken at the root of the notch of one of the samples water quenched from the beta phase region and tested at 20°C. The raised overall tear pattern, fine acicular-like tear ridges, and large facets, are quite reminiscent of observations made of the tensile fractures for this heat treatment. The fracture surface of the same acicular microstructure, when tested at 100°C, exhibits the features shown in Figure 40, at the notch root. The overall size of the fractographic features has not changed. However, there is significantly greater amount of subtle tear ridges and patterns present throughout the fracture. In addition, those regions of circular shaped dimples are larger and more numerous than those observed in the lower test temperature samples. This rather graphic difference in the

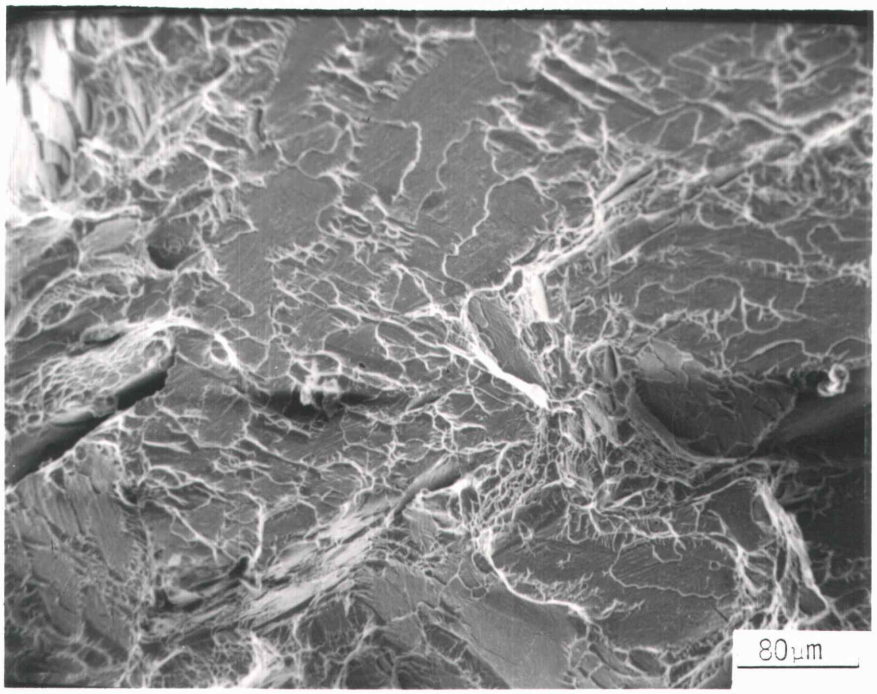

Figure 39. Impact fracture of sample water quenched from the beta phase field, taken at the root of the notch. Sample was tested at 20°C, 200X.

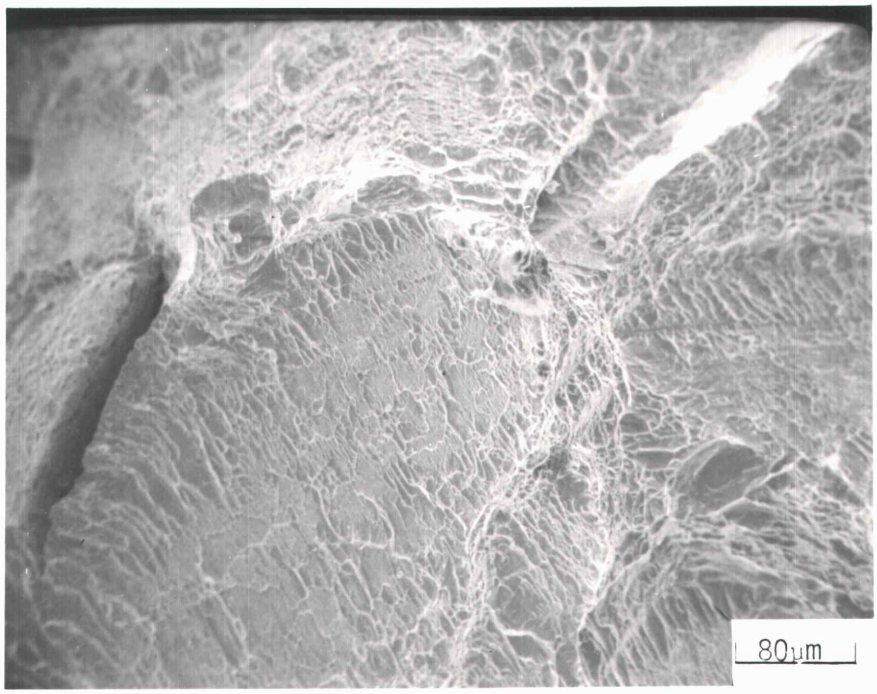

Figure 40. Impact fracture of sample with same microstructure as Fig. 39, but tested at 100°C. Note increased evidence of tear. Location is at root of notch, 200X.

degree of tearing was also observed in the samples air cooled from the beta field. Figure 41, fractured at 20°C, shows some elongated dimples coupled with areas of shallow circular dimples, on the larger faceted features. The 100°C fractured surface for this same microstructure, shown in Figure 42, exhibits an extensive network of tear ridge patterns throughout the larger facets. The regions of circular dimples seem to have enlarged considerably over that of the 20°C fracture. None of the other samples observed exhibited this radical change in failure mechanism with temperature.

SUMMARY OBSERVATIONS OF FRACTURES:

In summary, the general fractographic features of the samples exhibiting good ductility in the tensile tests and energy values comparable to the annealed material in the impact test, were characterized by fractures displaying large elongated dimples and tear ridge patterns. The samples water quenched or air cooled from the beta phase region tended to yield coarse fracture facets containing subtle tear ridges and networks indicative of the acicular nature of their microstructures. In these particular samples, increasing the temperature of the impact test produced a greater amount of tearing visible on the fracture surfaces. The regions of shallow circular dimples observed in most of the fractures seemed to be related to the amount of beta phase present in the microstructure. This feature was noted in samples containing both an acicular and intergranular form of the beta phase. The presence of elongated dimples in the tensile fracture of the sample furnace cooled from the beta region was inconsistent with the low tensile ductility

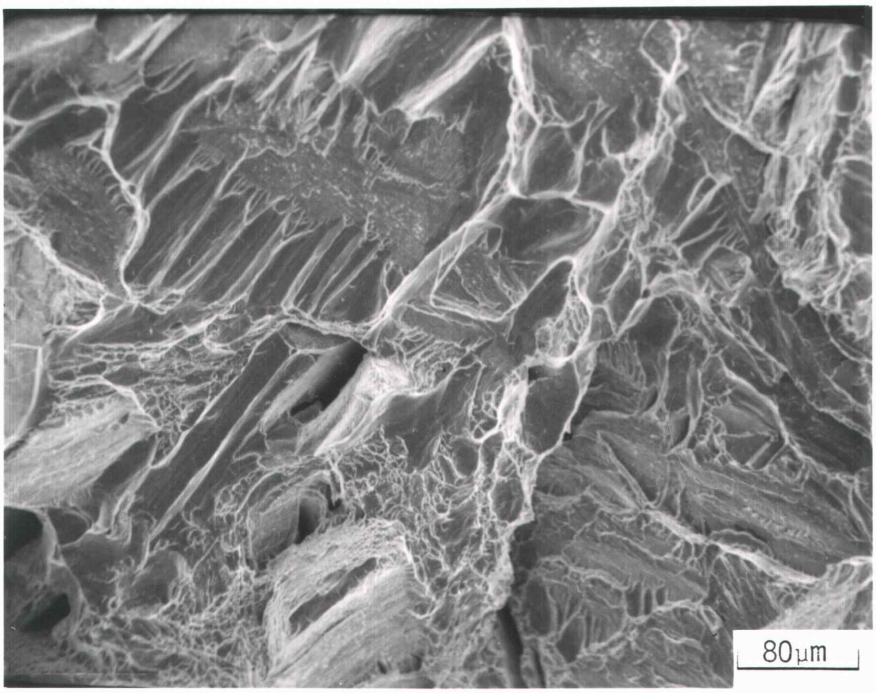

Figure 41. Impact fracture surface of sample air cooled from the beta phase region and tested at 20°C, taken at root of notch, 200X.

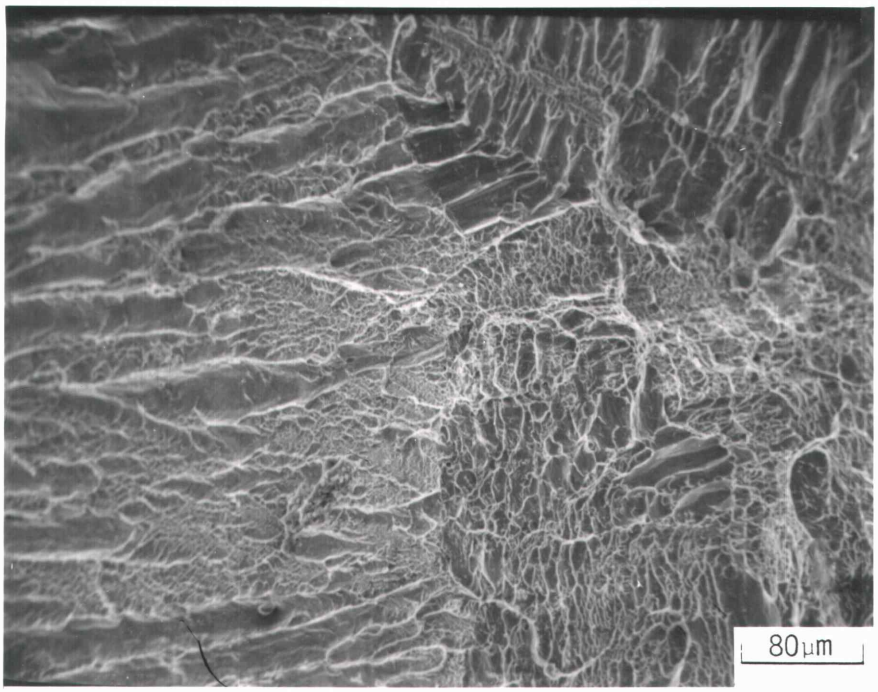

Figure 42. Impact fracture surface from sample with same microstructure as Fig. 41, but tested at 100°C, 200X.

displayed by these samples. The characteristics of the fracture were, however, in line with the microstructure observed earlier.

VII. DISCUSSION

Perhaps the most interesting outcome of this study is the revelation that the room temperature fracture toughness characteristics of commercial purity titanium can be altered, and, in fact, improved by heat treatment. In addition, the previously established contention that unalloyed grades of titanium would not experience improvements in mechanical properties with heat treatment is also not exactly correct. Although heat treating in the beta phase region produced significantly higher ultimate and yield strengths, there was a considerable sacrifice in ductility. This ductility loss may be related to the presence of iron, although the embrittling mechanism is not understood. In the case of fracture propagation during impact, however, heat treating in the beta phase region had a definite beneficial effect, especially with the slower cooling rates. For these structures, a greater percentage of the total energy absorbed by the sample was expended in propagating the initiated crack across the sample thickness. The greater energy absorbing fracture process, over that of the annealed equiaxed microstructures, appears to be related to the acicular nature of the beta quenched alpha phase. The increase in tear energy, however, seems to run opposite to that of the relative size of the acicular needles, with the largest tear energy percentage of the total energy displayed by the samples furnace cooled from the beta phase field. The same characteristic of higher tear energies seems to also predominate those microstructures containing both equiaxed and transformed alpha phase morphologies.

This latter tendency is in spite of the fact that only the water quenched samples contain any acicular nature at all, with the other two slower cooling rates exhibiting predominantly alpha grains and localized regions of beta phase and/or TiFe.

The increased tear energy of these non-acicular structures over that of the annealed material does not seem to be related to a grain size enlargement. Although it has been established in the past that an increase in grain size had a modest effect on impact values, these analyses examined only the total energy figures and were likely concerned with grain size differences much greater than those observed here[14].

It seems likely that the initial increase in tear energy percentages with the acicular microstructures is at least in part attributed to the increased amount of crack bifurcation noted in several titanium alloys by numerous authors[15,16]. The structure resulting from water quenching from the two phase region seems to be a close duplication to the microstructure produced by heat treating the alloy Ti-6Al-4V near the beta transformation temperature and water quenching. In both instances, a significant amount of acicular structure exists containing both the alpha and beta phases, in combination with localized areas of equiaxed alpha phase. In the case of Ti-6Al-4V, the equiaxed alpha seems to contribute to maintaining the ductility of the material at the higher toughness values. This same toughening mechanism and phase distribution must be, in part, responsible for the greater tear energies observed here.

The above mentioned increases in tear energy and redistribution of the portions of the total impact energy are not evident when one examines

only the total energy values. The total impact energy is significantly lower for the samples water quenched and air cooled from the beta phase field. The samples furnace cooled from the beta region and all of the mixed phase samples generally have about the same to somewhat less of the total energy as that of the annealed material. It is in the energy discriminating characteristics of the instrumented impact test that one realizes its true analytical value.

The mixed phase samples seem to display an additional anomaly when one examines the spread in strength values between their respective ultimate and yield strengths. In the samples quenched from the beta phase field, both the yield and ultimate strengths are elevated giving the same approximate strength difference between these two properties as that observed in the annealed material. The mixed phase samples, however, exhibit lower yield strength values than those of the annealed samples, while their ultimate strength values are less variable in comparison to the annealed properties. The increased energy required for failure after general yielding signifies an increased amount of work hardening. The increase in work hardening cannot be the result of simply alpha phase morphology, because as mentioned before, only the water quenched samples exhibited an acicular nature in part of the microstructure. Under the slower cooling of the air cool and furnace cool, it becomes possible that some type of precipitational mechanism is occurring as the material seeks to approach equilibrium. The formation of the compound TiFe might be exhibiting its presence by interfering with slip. However, the tendency of iron to stabilize the beta phase would seem to indicate that any iron compound precipitates

would like be adjacent to those beta regions in the microstructure. Again, with the exception of the water quenched samples, the percentage presence and general distribution of the beta phase in the slower cooled samples seems to preclude any widespread precipitational effect.

The coarser structures of the slower cooled mixed phase samples would actually be approaching the conditions of the annealed structure. From the standpoint of stored lattice energy, these two heat treatments would seem to reduce it, possibly to levels below that of the starting material. The actual mechanism of this work hardening phenomena needs to be examined further with regard to the role that microstructure plays in its development.

The variation of impact energy with temperature for both iodide titanium and commercial purity grades has been well documented. In those investigations involving the very pure iodide titanium, the general results indicated only a slight sensitivity to temperature variations from -200°C to 50°C and no evidence of any type of ductile-brittle transition, as observed in steels[17,18,19,20]. These same investigators noted a two to three fold increase in impact values between test temperatures of 50°C and 100°C. These energy increases seemed to be characteristic of not only the high purity titanium, but also commercial purity grades and alloys with small amounts of aluminum. However, the chemical content of the major impurity elements were significantly less than in this study. In addition, when these higher purity samples were quenched from the beta phase field, the resultant transformed structure was generally serrated and did not approach the acicularity observed in

the present study. When material of a higher impurity content was tested, information is generally lacking in impact energies of the Widmanstätten type structure.

A significant development noted in this study, in the samples containing the acicular alpha-beta microstructure, either as a major or secondary microstructural constituent, is that this type of structural form is very sensitive to test temperature within the range of 20°C to 100°C. Temperature transitions producing sevenfold increases in total energy values were noted in some instances. This is in striking contrast to the nominal 10% to 25% increases in those microstructures that did not exhibit any acicularity. This particular increase in impact energy with acicularity is not likely to be attributed solely to greater tear energy values since the percentage of tear energy in all of these samples did not vary nearly as much as in the samples tested at 20°C. However, the relative values of the tear energy percentages were greater than that of the 20°C tests, and the individual tear energies were also somewhat greater than those of the lower test temperature. The proportionate increases in both the initiation energies and tear energies at the increased test temperature are responsible for diminishing the variations in tear energy percentages observed in the 100°C tests.

The highest energies observed in the samples water quenched from the two phase region and tested at 100°C indicate the desirability of exploiting this type of microstructure in slightly elevated temperature applications where material toughness is a significant design consideration. In similar circumstances, it appears that in elevated temperature applications of cast commercial purity titanium, an increase in

toughness over that of lower temperatures should be expected. This same toughness benefit would also apply to welds made on either cast or wrought unalloyed grades, to the point of exceeding the bulk material toughness in the latter case. It appears that any heat treatment and cooling rate that is conducted near the alpha-beta phase transformation temperature or within the two phase region, will be beneficial to both tensile properties and toughness, without any sacrifices in ductility. In addition, slightly elevated temperature applications should immediately smooth out the variations in properties resulting from local microconstituent proportion changes, yielding more predictable and reproducible properties.

The observation of a fairly constant value for both the elastic energy and pop-in crack initiation energies in the impact tests, independent of both the microstructure and testing temperature, indicates that this type of testing is sensitive to material properties. Those differences observed in the other portions of the energy values would then appear to be truly representative of toughness dependency upon microstructure. It is significant to note that although alpha phase morphology must obviously change the fracture propagation characteristics, the actual fracture initiation event is solely dependent on the material. The formation of an infinitely small crack is directly related to the energy requirements for breaking primary bonds within the metal lattice. It is then consistent that this particular energy requirement should be independent of the macroscopic phase morphology as is observed in these tests. The inferred resemblance of this analysis to that of plane strain fracture toughness as a universal material pro-

perty cannot be assumed. In the latter instance, an attempt is made to isolate any geometrical or size dependency upon the fracture toughness, but the resulting values are generally macroscopic in nature and thus highly sensitive to microstructure. A smilar examination of the crack initiation or pop-in energy in plane strain fracture toughness testing, however, should yield similar values independent of any microstructural alteration.

The shortcomings of this study are readily apparent. A more comprehensive examination needs to be made of the temperature dependence of impact energy for the acicular and mixed phase forms of commercial purity titanium. Correlations need to be done with existing data that encompass a broader range of temperatures. A more complete characterization of the ductile-brittle transition may provide some understanding into why this particular phase morphology is so temperature sensitive. In addition, there are many questions with regard to the actual structural make-up of these particular microstructures. The presence and formation mechanism of TiFe needs to be determined such that its role in the structural dependence of impact energy can be ascertained. Finally, an analysis should be made of whether it is TiFe or some other precipitate or phenomena that is causing an increase in work hardening for samples slow cooled from the two phase region.

VIII. CONCLUSIONS

The following conclusions can be drawn from the results and observations of this investigation:

1. The phase composition of commercial purity titanium can be altered by heat treatment with a general improvement in strength and sometimes impact toughness, although in some instances accompanied by a drop in ductility.
2. In particular, the development of an acicular microstructure tends to increase the percentage tear energy in the slower cooled samples tested at 20°C, and in all of the acicular samples tested at 100°C.
3. Those samples quenched from the two phase region exhibit an increased amount of work hardening over the annealed material. This greater work hardening cannot be attributed to any precipitational strengthening mechanism observed in this study.
4. Although the annealed material and slow cooled mixed phase samples displayed only a modest increase in impact strength when tested at 100°C, those samples with an acicular microstructure were very sensitive to test temperature, with increases in energy as great as sevenfold when the test temperature was increased from 20°C to 100°C.
5. The greater impact toughness of the acicular type microstructures when tested at 100°C was well correlated with a significant increase in the amount of tear visible on the fracture surfaces.

BIBLIOGRAPHY

1. C. M. Craighead, G. A. Lenning, and R. I. Jaffee, Transactions of the AIME 194 (1952) 1317-1319.

2. G. A. Lenning, C. M. Craighead, and R. I. Jaffee, Transactions of the AIME 200 (1954) 367-376.

3. L. O. Odinokova, Physics of Metals and Metallography 35 (1973) 121-125.

4. L. P. Odinokova and B. A. Brusilovskiy, Physics of Metals and Metallography 31 (1971) 41-45.

5. J. C. Williams, Titanium Science and Technology, Plenum Press, New York (1973) 1433-1494.

6. R. I. Jaffee, Titanium Science and Technology, Plenum Press, New York (1973) 1665-1693.

7. M. J. Blackburn, The Science, Technology, and Application of Titanium, Pergamon Press, New York (1970).

8. R. I. Jaffee and I. E. Campbell, Transactions of the AIME 185 (1949) 646-654.

9. W. D. Bennett, Canadian Journal of Technology 32 (1954) 167-173.

10. C. M. Craighead, O. W. Simmons, and L. W. Eastwood, Transactions of the AIME 188 (1950) 485-513.

11. R. I. Jaffee, H. R. Ogden, and D. J. Maykuth, Transactions of the AIME 188 (1950) 1261-1266.

12. ASTM Standards; Metals-Physical, Mechanical, Corrosion Testing, Part 10, American Society for Testing and Materials, Philadelphia (1977) 154-173.

13. ASTM Standards; Metals-Physical, Mechanical, Corrosion Testing, Part 10, American Society for Testing and Materials, Philadelphia (1977) 230-246.

14. A. D. McQuillan and M. K. McQuillan, Titanium, Academic Press Inc., New York (1956).

15. G. R. Yoder, L. A. Cooley, and T. W. Crooker, Metallurgical Transactions 8A (1977) 1737-1743.

16. R. E. Lewis and F. A. Crossley, Correlation of Microstructure with Fracture Toughness Properties in Metals, Parts 1 and 2, Report LMSC-D454884, Lockheed Missiles and Space Company, Inc., Sunnyvale (January, 1975).

17. F. C. Holden, H. R. Ogden, and R. I. Jaffee, Transactions of the AIME 197 (1953) 238-242.

18. R. I. Jaffee, F. C. Holden, and H. R. Ogden, Transactions of the AIME 200 (1954) 1282-1290.

19. Von O. Rudiger and W. Knorr, Technische Mitteilungen Krupp 14 (1956) 105-113.

20. B. K. Vul'f and S. A. Yudina, Physical Metallurgy of Titanium, National Aeronautics and Space Administration, Washington, D. C. (1965).

21. M. Grumbach, M. Prudhomme, and G. Sanz, Revue de Metallurgie 66 (1969) 271-281.

22. D. R. Ireland, Procedures and Problems Associated with Reliable Control of the Instrumented Impact Test, Report TR 73-25R, Effects Technology, Inc., Santa Barbara (January, 1974).

APPENDIX

APPENDIX A

Energy Calculations from the Load-Time Plots of an Instrumented Impact Test

For a drop tower type of impact test, the total test energy available before test initiation is a function of the total drop mass, including the instrumented tup, m, and the effective drop height, h, to the sample. The pretest potential energy is then,

$$E_o = (\frac{W}{g})gh \qquad (1)$$

where W is the total weight of the drop hammer and assembly in kilograms, and g is the acceleration due to gravity, 9.81 m/sec^2. Upon release of the drop weight, the potential energy becomes kinetic energy. If the drop weight at this point is considered a free falling body, the energy is,

$$E_o = \tfrac{1}{2}(\frac{W}{g})V_o^2 \qquad (2)$$

where V_o is the velocity in m/sec just before impact, with W and g having the same designations as before. Equation 1 and 2 above, yield,

$$W(h) = \tfrac{1}{2}\left(\frac{W}{g}\right)V_o^2 \qquad (3)$$

where,

$$V_o^2 = 2gh \qquad (4)$$

or

$$V_o = \sqrt{2gh} \qquad (5)$$

The energy absorbed by the sample during the impact test is represented by the change in kinetic energy of the drop weight, or,

$$\Delta E = E_o - E_f \qquad (6)$$

where E_f is the kinetic energy of the drop weight at time t after contact with the specimen. If the initial and final energies of the drop weight are represented as before, then,

$$\Delta E = \tfrac{1}{2}\left(\frac{W}{g}\right)(V_o^2 - V_f^2) \qquad (7)$$

If the momentum of the drop weight is considered, then the change in momentum can be expressed as,

$$dP = F\,dt \qquad (8)$$

where F is the force of the weight, and t is some time after initial

specimen contact. The total momentum then, is,

$$P = \int_0^t F \, dt \qquad (9)$$

This integral can be equated to the change in velocity,

$$\int_0^t F \, dt = \frac{W}{g}(V_o - V_f) \qquad (10)$$

This same integral, when multiplied by the initial velocity, V_o, represents the area under the load-time plot and, therefore, the energy absorbed by the sample assuming a constant velocity. This energy is designated E_a,

$$E_a = -V_o \int_0^t F \, dt \qquad (11)$$

which is equivalent to,

$$E_a = -mV_o(V_f - V_o) \qquad (12)$$

If the actual energy absorbed by the sampe, E_c, is determined from the integral of the force time curve and an instantaneous velocity V, it must be equivalent to the change in kinetic energy. That is,

$$E_c = -\int_0^t FV \, dt = -\tfrac{1}{2}m(V_f^2 - V_o^2) \qquad (13)$$

where V_f is the velocity after the impact event. Now, since the initial

energy is,

$$E_o = \tfrac{1}{2}mV_o^2 \qquad (14)$$

the absorbed energy is the summation of the difference between the instantaneous velocity and the initial velocity minus the initial energy,

$$E_c = -\int_0^t F(V - V_o)\,dt - \int_0^t F\,V_o\,dt \qquad (15)$$

then,

$$E_c = -\int_0^t F(V - V_o)\,dt - E_a \qquad (16)$$

To get the integral in a more useful form with E_a, E_c, and E_o, we first multiply by the initial energy,

$$2E_o(E_c - E_a) = -m^2V_o^2 \int_{V_o}^{V_f} (V - V_o)g\,dt \qquad (17)$$

but gdt is equivalent to dV, so,

$$2E_o(E_c - E_a) = -m^2V_o^2 \int_{V_o}^{V_f} (V - V_o)\,d(V - V_o) \qquad (18)$$

$$2E_o(E_c - E_a) = -m^2V_o^2(V_f - V_o)^2/2 \qquad (19)$$

$$4E_o(E_c - E_a) = -m^2V_o^2(V_f - V_o)^2 \qquad (20)$$

$$= -E_a^2$$

therefore;

$$E_c - E_a = - \frac{E_a^2}{4E_o} \qquad (21)$$

$$E_c = E_a - \frac{E_a^2}{4E_o} \qquad (22)$$

or,
$$E_c = E_a\left(1 - \frac{E_a}{4E_o}\right) \qquad (23)$$

This comprehensive derivation is based upon the original relationship developed by Grumbach, et al.[21] and presented by Ireland[22].